Operator formalism for double quantum NMR*

S. Vega[†] and A. Pines[‡]

Department of Chemistry and Materials and Molecular Research Division, Lawrence Berkeley Laboratory, University of California, Berkeley, California 94720

(Received 16 November 1976)

An operator formalism is presented which conveniently treats the interaction of a spin-1 nucleus with a weak radio frequency field. The Hamiltonian in the rotating frame is $\mathcal{H} = -\Delta\omega\ I_z - \omega_1 I_x + (1/3)\omega_Q \times [3I_z^2 - I(I+1)]$, where $\Delta\omega$ is the resonance offset ($\Delta\omega = \omega_0 - \omega$), ω_1 is the intensity of the rf field, and ω_Q is the quadrupolar splitting. Nine fictitious spin$-1/2$ operators, $I_{p,i}$ where $p = x,y,z$ and $i = 1,2,3$, are defined where p refers to the transition between two of the levels and i the Cartesian component. The operators, which are the generators of the group $SU(3)$, satisfy spin-1/2 commutation relations $[I_{p,j}, I_{p,k}] = i\ I_{p,l}$, where $j,k,l = 1,2,3$ or cyclic permutation. Thus each p defines a three-dimensional space termed p space. For irradiation near one of the quadrupolar satellites, for example, $\Delta\omega = \omega_Q + \delta\omega$ with $\delta\omega$, $\omega_1 \ll \omega_Q$, it is shown that the effective Hamiltonian can be written $\mathcal{H} \approx -\delta\omega I_{x,3} - \sqrt{2}\,\omega_1 I_{x,1}$, i.e., a fictitious spin-1/2 Hamiltonian in x space with effective magnetogyric ratio γ along the 3 (resonance offset) axis and $\sqrt{2}\ \gamma$ along the 1 (rf field) axis. For irradiation near the center we can effect double quantum transitions between $m = \pm 1$. The formalism allows us to write the effective operators for these transitions. For example, if we take $\Delta\omega = \delta\omega$ again with $\delta\omega$, $\omega_1 \ll \omega_Q$ we find the effective double quantum (DQ) Hamiltonian $\mathcal{H}_{\mathrm{DQ}} \approx -2\ \delta\omega\ I_{z,1} - (\omega_1^2/\omega_Q)\ I_{z,3}$. Thus the z space is referred to as the double quantum frame with effective magnetogyric ratio 2γ along the 1 (resonance offset) axis and $(\omega_1/\omega_Q)\gamma$ along the 3 (rf field) axis. The limiting expressions are compared with exact calculations for arbitrary ω_1 done by high speed computer. The theory is applied to various cases of irradiation including our previously reported technique of Fourier transform double quantum NMR. Various pulse sequences for preparing, storing, and maintaining the evolution of double quantum coherence are analyzed for single crystal and polycrystalline samples. Finally, the effects of rf phase on the double quantum phase are presented briefly, and the possibility of double quantum spin locking is analyzed.

I. INTRODUCTION

One of the most familiar and useful descriptions of pulsed NMR experiments is in terms of the evolution of a magnetization vector in the rotating frame.[1] Often, in such experiments, a resonant radio frequency pulse brings the spin eigenfunctions into coherent superposition, creating a transverse magnetization which evolves in a free induction decay (FID) yielding on Fourier transformation an NMR absorption spectrum. For noninteracting spin-$\frac{1}{2}$ nuclei this description is complete, but may not be for spin-1 or greater or for interacting spins. In particular, we have been interested in the case of spin-1 such as deuterium, where it was shown recently[2,3] that states of the system can be created by double quantum transitions which cannot be described by a single three-dimensional vector. Such cases are important and have allowed us for the first time an approach to overcoming the large deuterium quadrupolar broadening and obtaining high resolution solid state Fourier transform NMR of deuterium.

The question which arises and is discussed in the present paper is whether we can provide a compact, convenient operator and vector picture for the description of this spin-1 pulsed NMR. To do this we need to develop an operator formalism for the possible single quantum and double quantum transitions in the system, such that the density operator and Hamiltonian of the system are described in terms of a set of basis operators with Cartesian commutation relations.[3] This would be a valuable supplement to the elegant three level Bloch equations developed by Brewer and Hahn.[4]

To make this more clear, let us consider a system of noninteracting I spins in an external magnetic field. The spin system can be defined by the spin density matrix ρ, which in the case of noninteracting spins has a dimension of $(2I+1)\times(2I+1)$. From the fact that there are $N = (2I+1)^2 - 1$ traceless independent Hermitian operators A_n, the density matrix can be expressed as

$$\rho(t) = \sum_{n=1}^{N} a_n(t) A_n + a_0 1, \tag{1}$$

where 1 is the unity matrix and the coefficients $a_n(t)$ can be obtained by solving the equation of motion for $\rho(t)$:

$$\frac{\partial}{\partial t}\rho(t) = -i[\mathcal{H}, \rho]. \tag{2}$$

$\mathcal{H}$ is the spin Hamiltonian of the system;

$$\mathcal{H} = -\omega_0 I_z - 2\omega_1 I_x \cos\omega t, \tag{3}$$

where $\omega_0 = \gamma H_0$ with H_0 magnetic field strength and $2\omega_1$ the rf irradiation strength at frequency ω. Using the high temperature approximation for the equilibrium form of ρ;

$$\rho_0 = \frac{1}{2I+1}\left(1 + \frac{\omega_0}{kT} I_z\right), \tag{4}$$

and representing the density matrix in the rotating frame

$$\rho^* = \exp(-i\omega I_z t)\,\rho\,\exp(i\omega I_z t), \tag{5}$$

the solution of Eq. (2) is

$$\rho = \exp[i(\Delta\omega I_z + \omega_1 I_x)t]\,\rho_0\,\exp[-i(\Delta\omega I_z + \omega_1 I_x)t]. \tag{6}$$

where we have dropped the asterisk on ρ. The most general form of this solution is easily obtained from the commutation relations between the angular momentum operators I_x, I_y, and I_z,

Copyright © 1977 American Institute of Physics

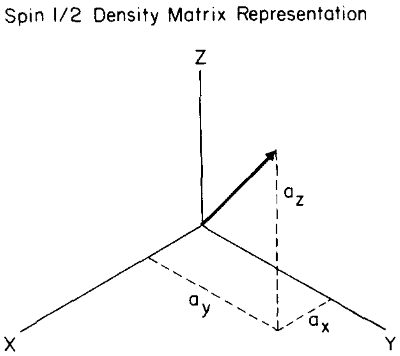

FIG. 1. For isolated spin-$\frac{1}{2}$ the density matrix can be written $\rho = a_x I_x + a_y I_y + a_z I_z$ ignoring the constant $a_0 1$ term. This is depicted schematically as a three-dimensional vector which is proportional to the magnetization.

$$\rho = \sum_{p=x,y,z} a_p(t) I_p + a_0 1, \tag{7}$$

and is depicted schematically in Fig. 1. It is therefore clear that for this case the spin system is defined by the coefficients of only three operators I_x, I_y, and I_z and that we do not need all $(2I+1)^2 - 1$ operators. This simplification also makes it possible to represent the density matrix in terms of a vector in a three-dimentional space with coordinates, a_x, a_y, and a_z. This vector describes the density matrix sufficiently and is proportional to the real magnetization vector in the rotating frame.

All these basic arguments are valid in the case that the main Hamiltonian $\mathcal{H}$ has only linear terms in the angular momentum operator. If we add any bilinear term to the Hamiltonian, the solution of Eq. (2) no longer has the simple form of Eq. (7) and the three angular momentum operators are not sufficient to describe ρ. For the particular case of $I = \frac{1}{2}$, these solutions are general for any interaction, because there are only three independent traceless Hermitian operators with dimension 2×2 (Pauli matrices). However for $I > \frac{1}{2}$ there are more than three and we must use them to describe the spin system in operational form. For our case we need to add electric quadrupolar interacactions to the Zeeman interactions in Eq. (3) and to define a new basis set of operators. The number of operators is determined by the spin value I, and they can be taken in many forms. Physically, the additional operators correspond to the possibility of operations other than pure rotations on the spin system, such as the production of normally forbidden transitions. In the next section we define a convenient set of operators for spin systems for $I = 1$ and show that they have a useful Cartesian representation. This particular choice is very helpful for the description of pure nuclear quadrupole resonance in solids[5] and it will be shown to be just as useful in the description of double quantum coherence and cross polarization experiments of deuterium NMR in solids. The main thrust of the theory is therefore to provide a formal basis for describing double quantum experiments. Other choices of operator basis sets are of couse possible.[5]

In Sec. III the Zeeman and the electric quadrupole Hamiltonian are represented in terms of these operators, and in Sec. IV the solution for the spin density matrix for different forms of the Hamiltonian is derived. The actual physical observables, the signal intensities and frequencies, are discussed in Sec. V, and the Fourier transforms of the signals observed in an NMR experiment are calculated.

In Sec. VI we present the results of central interest based on the formalism of the previous sections. We consider the case of double quantum coherence and its detection. It is shown that in an appropriate limit the evolution of the system can be described in terms of rotations of a vector in a fictitious three-dimensional space, a subspace of the full set of operators introduced previously. The physical significance of this frame and its transformations to the observed rotating frame are discussed. The basic structure of Secs. IV–VI is therefore logically broken into the following steps: preparation→evolution→detection. Finally, applications of the theory to deuterium NMR in single crystals and polycrystalline samples are illustrated in Sec. VII.

II. FICTITIOUS SPIN-½ OPERATORS

Let us now consider a system of noninteracting spins $I = 1$ in an external magnetic field with a nonvanishing electric quadrupole interaction. As was mentioned before, the density matrix for such a system cannot be described by only three angular momentum operators and we have to define a set of eight independent traceless Hermitian operators. The set we select has particular commutation relations between the individual operators. The matrix representation of the operators in the basis set of the eigenfunctions of I_z^2 consists of the fictitious spin-half operators and to the generators of the group $SU(3)$.[6] The operators in terms of the three linear angular momentum operators are given by

$$\begin{aligned} &I_{x,1} \equiv \tfrac{1}{2} I_x, && I_{y,1} = \tfrac{1}{2} I_y, && I_{z,1} = \tfrac{1}{2} I_z, \\ &I_{x,2} = \tfrac{1}{2}(I_y I_z + I_z I_y), && I_{y,2} = \tfrac{1}{2}(I_z I_x + I_x I_z), && I_{z,2} = \tfrac{1}{2}(I_x I_y + I_y I_x), \\ &I_{x,3} = \tfrac{1}{2}(I_z^2 - I_y^2), && I_{y,3} = \tfrac{1}{2}(I_x^2 - I_z^2), && I_{z,3} = \tfrac{1}{2}(I_y^2 - I_x^2). \end{aligned} \tag{8}$$

For reasons of symmetry we defined nine operators which are dependent through the equality

$$I_{x,3} + I_{y,3} + I_{z,3} = 0. \tag{9}$$

The most important property of these operators is that $I_{p,1}$, $I_{p,2}$, and $I_{p,3}$ behave like the Cartesian angular momentum operators I_x, I_y, and I_z for all three possible p's; $p = x, y, z$;

namely,

$$[I_{p,1}, I_{p,2}] = i I_{p,3} \tag{10}$$

or cyclic permutation of 1, 2, 3, and therefore

$$e^{-i\theta I_{p,1}} I_{p,2} e^{i\theta I_{p,1}} = (I_{p,2} \cos\theta + I_{p,3} \sin\theta). \tag{11}$$

The form of the operators and their transformations are summarized in Table I, and the matrix representation of these operators for $I = 1$ is shown in Table II.

The two indices p, i in $I_{p,i}$ indicate that for each p we have a subspace $i = 1, 2, 3$ with spin-$\frac{1}{2}$ transformation

TABLE I. Fictitious spin-$\frac{1}{2}$ operators in terms of spin-1 operators.

Definitions

$$\left.\begin{aligned}&I_{p,1}=\tfrac{1}{2}I_p\\&I_{p,2}=\tfrac{1}{2}(I_qI_r+I_rI_q)\\&I_{p,3}=\tfrac{1}{2}(I_r^2-I_q^2)\end{aligned}\right\}\ p,q,r=x,y,z\text{ or cyclic permutation}$$

Commutation relations

$$\left.\begin{aligned}&[I_{p,i},I_{p,j}]=iI_{p,k}\\&[I_{p,1},I_{q,2}]=-\frac{i}{2}I_{r,2}\\&[I_{p,2},I_{q,1}]=-\frac{i}{2}I_{r,2}\\&[I_{p,2},I_{q,2}]=-\frac{i}{2}I_{r,1}\\&[I_{p,1},I_{q,3}-I_{r,3}]=0\end{aligned}\right\}\ \begin{aligned}&i,j,k=1,2,3\text{ or cyclic permutation}\\&p,q,r=x,y,z\text{ or cyclic permutation}\end{aligned}$$

Linear dependence

$$I_{x,3}+I_{y,3}+I_{z,3}=0$$

Fictitious spin-$\frac{1}{2}$ transformations

$$U_{p,i}^{\dagger}I_{p,j}U_{p,i}=\cos\theta I_{p,j}+\sin\theta I_{p,k}$$

$$U_{p,1}^{\dagger}I_{q,1}U_{p,1}=\cos\theta/2\,I_{q,1}+\sin\theta/2\,I_{r,1}$$

$$U_{p,1}^{\dagger}I_{q,2}U_{p,1}=\cos\theta/2\,I_{q,2}-\sin\theta/2\,I_{r,2}$$

$$U_{p,2}^{\dagger}I_{q,1}U_{p,2}=\cos\theta/2\,I_{q,1}-\sin\theta/2\,I_{r,2}$$

$$U_{p,2}^{\dagger}I_{q,2}U_{p,2}=\cos\theta/2\,I_{q,2}-\sin\theta/2\,I_{r,1}$$

with

$$U_{p,i}=\exp(i\theta I_{p,i})$$

$p,q,r=x,y,z$ or cyclic permutation

$i,j,k=1,2,3$ or cyclic permutation

properties, thus the name fictitious spin-$\frac{1}{2}$ operators.[7] Thus each p defines a three-dimensional space which we term the p space. In particular, for reasons which will become clear, the z space is termed the double quantum space. In many physically realistic situations the spin system will evolve with no transitions between the p spaces and will consist of rotations in one three-dimensional space.

Now, using these operators we rewrite the Hamiltonian and the spin density matrix of the spin system. If we consider a Zeeman and quadrupole Hamiltonian we have

$$\begin{aligned}\mathcal{H}&=-\omega_0I_z+\tfrac{1}{3}\omega_Q[3I_z^2-I(I+1)]\\&=-2\omega_0I_{z,1}+\tfrac{2}{3}\omega_Q(I_{x,3}-I_{y,3}),\end{aligned}\tag{12}$$

where $\omega_0=\gamma_IH_0$ is again the external magnetic field strength in angular frequency units, and

$$2\omega_Q=\frac{e^2qQ}{2I(2I-1)}[\tfrac{1}{2}(3\cos^2\theta-1)+\eta\sin^2\theta\cos2\phi]$$

is the quadrupole interaction strength truncated with respect to the direction of the magnetic field ($\omega_Q\ll\omega_0$).[1] In the fictitious spin-$\frac{1}{2}$ formalism, the two terms in the Hamiltonian of Eq. (12) are commutative, because of the general rule

$$[I_{p,i},\ I_{q,3}-I_{r,3}]=0\quad p,q,r=x,y,z\quad i=1,2,3,\tag{13}$$

an important relationship which will be used later many times; it is particularly important for cross polarization experiments, in which case they form the two constants of the motion.[8] At high temperatures, a possible representation of the density matrix in terms of the nine operators,

$$\rho=\sum_{i=1}^{3}\sum_{p=x,y,z}a_{p,i}(t)\,I_{p,i}+a_01,\tag{14}$$

is conveniently described in terms of three coordinate systems according to the three goups of three operators defined by p in Eq. (10). In Fig. 2 we demonstrate pictorially this representation. From the definitions of the operators, only the $(p,1)$ axes correspond to the observable angular momentum expectation values $\langle I_x\rangle$, $\langle I_y\rangle$, and $\langle I_z\rangle$. It will be shown in the next section that we can connect each coordinate system to one of the three transitions in the three level system of spin $I=1$ in the rotating frame. The properties of the operators and the simple transformation rules in Tables I and II will be used in the following sections to describe the spin system in the most convenient way. For completeness we give the expressions of our operators in terms of the irreducible tensor representation components T_{lm} of the angular momentum operators of first and second rank[9]:

$$\begin{aligned}&I_{x,1}=\frac{\sqrt{2}}{4}(T_{11}-T_{1-1}), &&I_{x,2}=-\frac{1}{2}(T_{21}-T_{2-1}),\\&I_{y,1}=-\frac{\sqrt{2}}{4}(T_{11}+T_{1-1}), &&I_{y,2}=\frac{1}{2}(T_{21}+T_{2-1}),\\&I_{x,3}=\frac{\sqrt{6}}{4}T_{20}+\frac{1}{4}(T_{22}+T_{2-2}), &&I_{y,3}=-\frac{\sqrt{6}}{4}T_{20}+\frac{1}{4}(T_{22}+T_{2-2}),\\&I_{z,1}=\frac{1}{2}T_{10},\quad I_{z,2}=-\frac{1}{2}(T_{22}-T_{2-2}), &&I_{z,3}=-\frac{1}{2}(T_{22}+T_{2-2}).\end{aligned}\tag{15}$$

In the description of our experiments of double quantum NMR, the T_{lm} are not convenient operators. We can see that the $I_{z,2}$ and $I_{z,3}$ operators are related to the double quantum transition states ($\Delta m=2$), while $I_{y,1}$, $I_{y,2}$ and $I_{x,1}$ and $I_{x,2}$ have matrix elements between the levels of the single quantum transitions ($\Delta m=1$). We can now discuss the spin Hamiltonian of a spin system with $I=1$ in terms of the operators of Table I and we

TABLE II. Matrix representation of the nine operators.

$I_{z,1}=\frac{1}{2}\begin{pmatrix}0&i&0\\-i&0&0\\0&0&0\end{pmatrix}$	$I_{z,2}=\frac{1}{2}\begin{pmatrix}0&1&0\\1&0&0\\0&0&0\end{pmatrix}$	$I_{z,3}=\frac{1}{2}\begin{pmatrix}1&0&0\\0&-1&0\\0&0&0\end{pmatrix}$
$I_{y,1}=\frac{1}{2}\begin{pmatrix}0&0&1\\0&0&0\\1&0&0\end{pmatrix}$	$I_{y,2}=\frac{1}{2}\begin{pmatrix}0&0&i\\0&0&0\\-i&0&0\end{pmatrix}$	$I_{y,3}=\frac{1}{2}\begin{pmatrix}-1&0&0\\0&0&0\\0&0&1\end{pmatrix}$
$I_{x,1}=\frac{1}{2}\begin{pmatrix}0&0&0\\0&0&1\\0&1&0\end{pmatrix}$	$I_{x,2}=\frac{1}{2}\begin{pmatrix}0&0&0\\0&0&-i\\0&i&0\end{pmatrix}$	$I_{x,3}=\frac{1}{2}\begin{pmatrix}0&0&0\\0&1&0\\0&0&-1\end{pmatrix}$

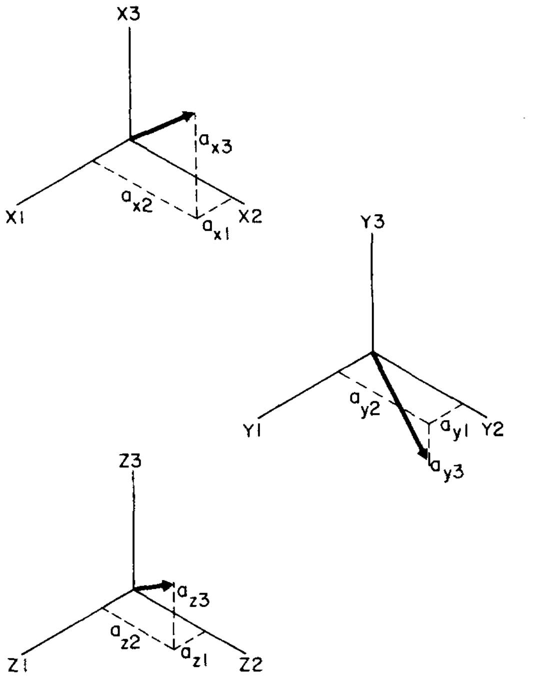

FIG. 2. For isolated spin-1, this figure depicts schematically the representation of the density matrix based on the nine fictitious spin-$\frac{1}{2}$ operators $I_{p,i}$ $p=x,y,z$ and $i=1,2,3$, i.e., $\rho=\sum_{p,i} a_{p,i} I_{p,i} + a_0 1$. The commas in p,i are suppressed in the figure for compactness. The state of the system is specified by the three vectors in the three p spaces, each of which corresponds to one two-level transition. In special cases where weak and selective rf irradiation is applied, the vectors may rotate independently in the three spaces. The z space ($z1, z2, z3$) is referred to as the double quantum space; $z1$ is related to I_z, the z magnetization, and $z2$, $z3$ are related to the double quantum coherence as explained in the text. $I_{p,i}$ have spin-$\frac{1}{2}$ commutation relations for $i=1,2,3$.

shall derive the different forms of this Hamiltonian for different situations of frequency and intensity of radio frequency irradiation.

III. HAMILTONIANS

The purpose of this section will be to represent the spin Hamiltonian of a spin system with spins $I=1$ in terms of the operators of Table I for several experimentally realistic situations. In general and with the definitions of Eq. (12), we write the Hamiltonian

$$\mathcal{H} = -\omega_0 I_z + \tfrac{1}{3}\omega_Q[3I_z^2 - I(I+1)] - 2\omega_1 I_x \cos\omega t \tag{16}$$

for the spin-1 nucleus with Zeeman and quadrupole coupling (see Fig. 3) where we allow for a rf irradiation field of strength of $2\omega_1$ and of frequency ω. With the assumption that $\omega_0 \gg \omega_Q$ it is common to represent the spin system in the rotating frame defined by the unitary transformation

$$U = \exp(-i\omega I_z t). \tag{17}$$

The Hamiltonian then becomes (suppressing rapidly oscillating terms)

$$\mathcal{H}^* = U^+\mathcal{H}U = -\Delta\omega I_z - \omega_1 I_x + \tfrac{1}{3}\omega_Q[3I_z^2 - I(I+1)], \tag{18}$$

where

$$\omega_0 - \omega = \Delta\omega.$$

Since we work from now on in the rotating frame, we suppress the asterisk. The Hamiltonian can now be written in terms of the operators of Table I:

$$\mathcal{H} = -2\Delta\omega I_{z,1} - 2\omega_1 I_{x,1} + \tfrac{2}{3}\omega_Q(I_{x,3} - I_{y,3}). \tag{19}$$

To emphasize the use of the new operators we shall discuss this Hamiltonian for different values of $\Delta\omega$, ω_1, and ω_Q. We shall show that by proper rotations this Hamiltonian assumes a convenient form which makes it easier to deal with. As a rule we shall always try to write $\mathcal{H}$ in terms of $I_{x,3}$, $I_{y,3}$, and $I_{z,3}$, because then it is possible to evaluate the behavior of the spin density matrix as a function of time analytically. This is analogous to the case of only Zeeman interaction in which we rotate the Hamiltonian in the rotating frame to a frame so that the Hamiltonian becomes proportional to I_z, i.e., the tilted rotating frame.[10] *Here we shall want the vectors along p, 3 in each of the p-frames.*

$\Delta\omega = 0$, $\omega_1 = 0$ *(at resonance, no irradiation).* The first case under consideration corresponds to a situation where there is not a rf field and the rotating frame is taken to be at frequency ω_0. Then

$$\mathcal{H} = +\tfrac{2}{3}\omega_Q(I_{x,3} - I_{y,3}) \tag{20a}$$

$$= \omega_Q I_{x,3} - \tfrac{1}{3}\omega_Q(I_{y,3} - I_{z,3}) \tag{20b}$$

$$= -\omega_Q I_{y,3} - \tfrac{1}{3}\omega_Q(I_{z,3} - I_{x,3}). \tag{20c}$$

The three expressions for $\mathcal{H}$ are identical and can be obtained by using the definitions of Table I. The reason for representing $\mathcal{H}$ in the three forms is that each expression has the form

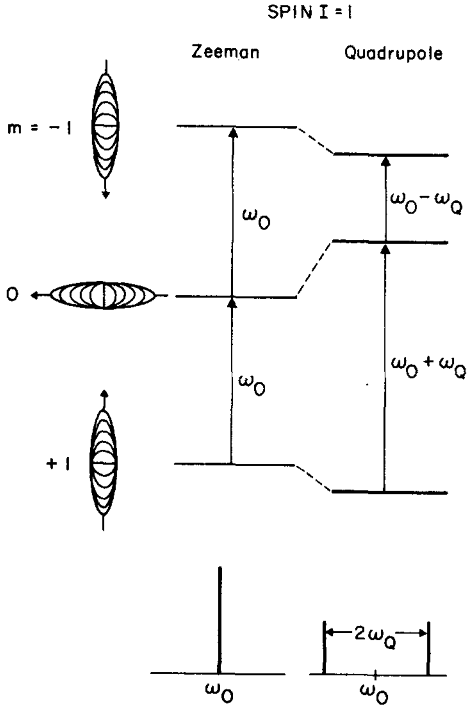

FIG. 3. Energy levels for quadrupolar spin-1 in high magnetic field. The quadrupolar interaction gives rise to two "allowed" transitions at frequencies $\omega_0 \pm \omega_Q$ where ω_0 is the Larmor frequency. The double quantum transition from $m=+1$ to $m=-1$ is unshifted, at ω_0.

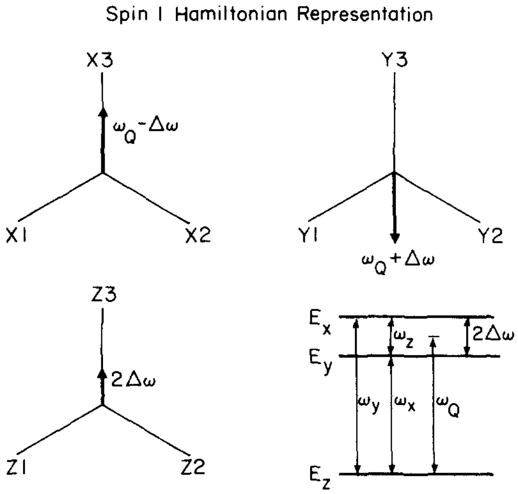

FIG. 4. Schematic representation of the quadrupole Hamiltonian $\mathcal{H}_T$ of Eqs. (24) and (25) in the three p spaces of the fictitious spin-$\frac{1}{2}$ operators $I_{p,i}$. The three vectors representing $\mathcal{H}_T$ correspond to the first terms in (24) and (25): a vector along $x3$ of magnitude $\omega_Q-\Delta\omega$ depicts the term of the form $(\omega_Q-\Delta\omega)I_{x,3}$ in (25). The three vectors in Fig. 2 representing the density matrix will rotate each around its $p3$ axis with a frequency ω_p, due to these $\mathcal{H}_T$ vectors. With the definition of ω_p in Eq. (26) we obtain $\omega_x=\omega_Q-\Delta\omega$, $\omega_y=-(\omega_Q+\Delta\omega)$, and $\omega_z=2\Delta\omega$. The bottom right of the figure depicts the energy scheme of $\mathcal{H}_T$ corresponding to the parameters of (26).

$$\mathcal{H}=\alpha_p I_{p,3}-\alpha_{qr}(I_{q,3}-I_{r,3}) \quad \text{with } p,q,r=x,y,z \text{ or cyclic permutation,} \tag{21}$$

a sum of two commuting operators [Eq. (13)]. These representations make it possible to obtain simply the solution of the equation of motion in the rotating frame for different initial density matrices:

$$\partial\rho/\partial t=-i[\mathcal{H},\rho]$$

For example, if $\rho(0)=I_x$, then we use (20b) to find

$$\begin{aligned}\rho(t)&=2e^{-i\mathcal{H}t}I_{x,1}e^{+i\mathcal{H}t}\\&=2e^{-i[\omega_Q I_{x,3}-(1/3)\omega_Q(I_{y,3}-I_{z,3})]t}\\&\quad\times I_{x,1}e^{i[\omega_Q I_{x,3}-(1/3)\omega_Q(I_{y,3}-I_{z,3})]}\\&=2e^{-i\omega_Q I_{x,3}t}e^{i(\omega_Q/3)(I_{y,3}-I_{z,3})t}\\&\quad\times I_{x,1}e^{-i(\omega_Q/3)(I_{y,3}-I_{z,3})t}e^{i\omega_Q I_{x,3}t}\\&=2e^{-i\omega_Q I_{x,3}t}I_{x,1}e^{i\omega_Q I_{x,3}t}\\&=2(I_{x,1}\cos\omega_Q t+I_{x,2}\sin\omega_Q t).\end{aligned}\tag{22}$$

The last step in Eq. (22) is calculated using the first commutation relation in Table I. The important properties of Eq. (20) will be used many times in calculating the evolution of the density matrix. The usefulness of these representations will become clear when we apply an rf field with small ω_1, where they maintain their form after a small fictitious spin-$\frac{1}{2}$ rotation.

$\Delta\omega\neq 0$, $\omega_1=0$ (*off resonance, no irradiation*).

When we consider the rotating frame with respect to a rotation frequency different from ω_0, then $\Delta\omega\neq 0$, and $\mathcal{H}$ becomes in the rotating frame

$$\mathcal{H}=-2\Delta\omega I_{z,1}+\tfrac{2}{3}\omega_Q(I_{x,3}-I_{y,3}).\tag{23}$$

To derive from this equation the general form of Eq. (21), we apply a transformation corresponding to a tilt of our coordinate system with the operator

$$U_{z,2}(\tfrac{1}{2}\pi)=\exp(i\tfrac{1}{2}\pi I_{z,2}).$$

The transformed (tilted Hamiltonian $\mathcal{H}_T$ can be calculated, realizing that $U_{z,2}$ operating on the first term of $\mathcal{H}$ will rotate it to $I_{z,3}$ and that it is commutative with the second term,

$$\mathcal{H}_T=U^{+}_{z,2}\mathcal{H}U_{z,2}=2\Delta\omega I_{z,3}+\tfrac{2}{3}\omega_Q(I_{x,3}-I_{y,3}).\tag{24}$$

Again we can rewrite $\mathcal{H}_T$ according to the definitions of $I_{p,3}$:

$$\begin{aligned}\mathcal{H}_T&=(\omega_Q-\Delta\omega)I_{x,3}-(\tfrac{1}{3}\omega_Q+\Delta\omega)(I_{y,3}-I_{z,3})\\&=-(\omega_Q+\Delta\omega)I_{y,3}-(\tfrac{1}{3}\omega_Q-\Delta\omega)(I_{z,3}-I_{x,3}).\end{aligned}\tag{25}$$

To obtain the expressions in Eq. (25) from Eq. (24) we use the following formalism: The Hamiltonian for the three level system of spins with $I=1$ can always be represented, after the proper tilt, by

$$\begin{aligned}\mathcal{H}_T&=(E_x-E_y)I_{z,3}-E_z(I_{x,3}-I_{y,3})=\omega_z I_{z,3}-E_z(I_{x,3}-I_{y,3})\\&=(E_y-E_z)I_{x,3}-E_x(I_{y,3}-I_{z,3})=\omega_x I_{x,3}-E_x(I_{y,3}-I_{z,3})\\&=(E_z-E_x)I_{y,3}-E_y(I_{z,3}-I_{x,3})=\omega_y I_{y,3}-E_y(I_{z,3}-I_{x,3}),\end{aligned}\tag{26}$$

where E_x, E_y, E_z are the energies of the eigenstates $|x\rangle$, $|y\rangle$, and $|z\rangle$ of $\mathcal{H}_T$. The expressions of the eigenstates of $\mathcal{H}_T$ in terms of the eigenstates of I_z in this tilted frame are

$$\begin{aligned}|x\rangle&=-\frac{1}{\sqrt{2}}(|+1\rangle-|-1\rangle);\\|y\rangle&=\frac{i}{\sqrt{2}}(|+1\rangle+|-1\rangle),\\|z\rangle&=|0\rangle.\end{aligned}\tag{27}$$

This can be derived from the definitions of $I_{p,3}$ and

$$\begin{aligned}I_{p,3}|p\rangle&\equiv\tfrac{1}{2}(I_r^2-I_q^2)|p\rangle=0,\\I_{q,3}|p\rangle&=\tfrac{1}{2}(I_p^2-I_r^2)|p\rangle=-\tfrac{1}{2}|p\rangle,\\I_{r,3}|p\rangle&=\tfrac{1}{2}(I_q^2-I_p^2)|p\rangle=\tfrac{1}{2}|p\rangle.\end{aligned}\tag{28}$$

This is depicted schematically in Fig. 4. From the matrix representation in Table II, we can see that the fact that the trace of $\mathcal{H}$ is zero corresponds here to

$$E_x+E_y+E_z=0.\tag{29}$$

$\Delta\omega=0$, $\omega_1\neq 0$ (*irradiation at resonance*).

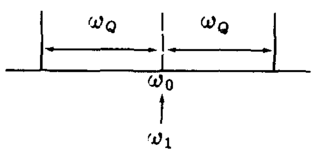

We now introduce the radio frequency irradiation field at frequency ω_0,

$$\mathcal{H}=-2\omega_1 I_{x,1}+\tfrac{2}{3}\omega_Q(I_{x,3}-I_{y,3}).\tag{30}$$

To find the tilt operator which will transform this Hamiltonian to the form of Eq. (26), we rewrite $\mathcal{H}$ again in the following way:

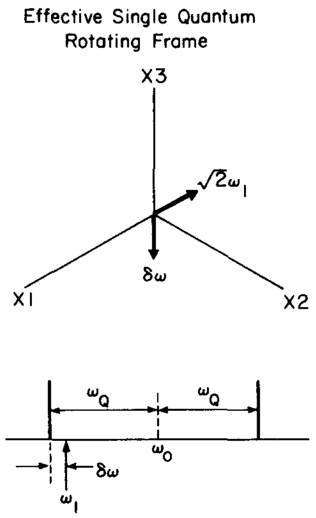

FIG. 5. When the system is irradiated near the frequency of the low field quadrupolar satellite $\omega_0 - \omega_Q$ such that $\delta\omega$, $\omega_1 \ll \omega_Q$, the effective Hamiltonian in a tilted frame defined in the text is given by $\mathcal{H}_T \approx -\delta\omega I_{x,3} - \sqrt{2}\omega_1 I_{x,1}$. Thus the Hamiltonian is that of a fictitious spin-$\frac{1}{2}$ in the three-dimentional x space, with effective magnetogyric ratio γ along $x, 3$ (the effective external field direction) and $\sqrt{2}\gamma$ along $x, 1$ (the effective applied rf field direction). The figure depicts this concept schematically. The term single quantum frame is used as a reminder that the irradiation is near one of the allowed transitions and involves normal single quantum effects.

$$\mathcal{H} = -2\omega_1 I_{x,1} + \omega_Q I_{x,3} - \tfrac{1}{3}\omega_Q (I_{y,3} - I_{z,3}). \tag{31}$$

We now tilt with the operator

$$U_{x,2}(\theta) = \exp(i\theta I_{x,2}),$$

with

$$\theta = \tan^{-1}(2\omega_1/\omega_Q).$$

The reason for writing Eq. (31) is now clear, because $I_{x,2}$ commutes with the third term and rotates the two first terms:

$$\mathcal{H}_T = U^{\dagger}_{x,2}\mathcal{H}\,U_{x,2} = +\,\omega_e I_{x,3} - \tfrac{1}{3}\omega_Q(I_{y,3} - I_{z,3})$$
$$= -\tfrac{1}{2}(\omega_e - \omega_Q) I_{z,3} + [\tfrac{2}{3}\omega_Q + \tfrac{1}{2}(\omega_e - \omega_Q)](I_{x,3} - I_{y,3}), \tag{32}$$

with

$$\omega_e = (4\omega_1^2 + \omega_Q^2)^{1/2}, \tag{33}$$

where we again used Eq. (26) to obtain the second expression. Clearly, in the last term of (32), $\omega_e - \omega_Q$ can be neglected.

For the case that $\omega_1 \ll \omega_Q$ Eq. (32) results in

$$\mathcal{H}_T = -(\omega_1^2/\omega_Q) I_{z,3} + \tfrac{2}{3}\omega_Q(I_{x,3} - I_{y,3}), \tag{34}$$

where we used

$$\tfrac{1}{2}[(4\omega_1^2 + \omega_Q^2)^{1/2} - \omega_Q] \simeq \omega_1^2/\omega_Q. \tag{35}$$

A similar result can be obtained by coherent averaging of $-\omega_1 I_x$ by $\mathcal{H}_Q$ when the approximation $\omega_1 \ll \omega_Q$ is valid.[11]

$\Delta\omega \neq 0$, $\omega_1 \neq 0$ (*general case*).

Finally, we shall discuss the case in which all terms of Eq. (19) are different from zero. In this case it is not simple to transform $\mathcal{H}$ to our desired form. However, for the most important situations where $\omega_1 \ll \omega_Q$ we can obtain the result with an approximation. We shall therefore discuss these cases separately in the following:

$\Delta\omega \sim \omega_Q$, $\omega_1 \ll \omega_Q$ (*irradiation near low satellite*).

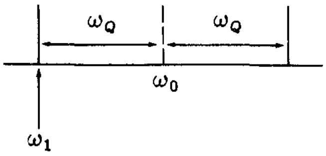

We start with an rf irradiation field about the frequency $(\omega_0 - \omega_Q)$. In this case the Hamiltonian becomes, with $\Delta\omega = \omega_Q + \delta\omega$ and $\delta\omega \ll \omega_Q$,

$$\mathcal{H} = -2(\omega_Q + \delta\omega) I_{z,1} + \tfrac{2}{3}\omega_Q(I_{x,3} - I_{y,3}) - 2\omega_1 I_{x,1}\,. \tag{36}$$

Tilting this Hamiltonian by $U_{z,2}(\frac{1}{2}\pi)$, we obtain [Table I and Eq. (25)]

$$\mathcal{H}_T = 2(\omega_Q + \delta\omega) I_{z,3} + \tfrac{2}{3}\omega_Q(I_{x,3} - I_{y,3})$$
$$-2\omega_1\left(\frac{1}{\sqrt{2}} I_{x,1} - \frac{1}{\sqrt{2}} I_{y,2}\right)$$
$$= -\delta\omega I_{x,3} - (\tfrac{4}{3}\omega_Q + \delta\omega)(I_{y,3} - I_{z,3}) - \sqrt{2}\omega_1 (I_{x,1} - I_{y,2})\,. \tag{37}$$

We now use the approximation $\omega_1 \ll \omega_Q$ to simplify the last term. In the last expression of Eq. (37) we realize that with the approximation $\omega_1 \ll \omega_Q$, the term $\sqrt{2}\omega_1 I_{y,2}$ can be neglected, yielding

$$\mathcal{H}_T \approx -\delta\omega I_{x,3} - \sqrt{2}\omega_1 I_{x,1} - (\tfrac{4}{3}\omega_Q + \delta\omega)(I_{y,3} - I_{z,3}). \tag{38}$$

This result has the form of a Zeeman interaction in the fictitious x-rotating frame (x space) with an rf field of $\sqrt{2}\omega_1$ intensity and an offset frequency of $\delta\omega$ as in Fig. 5. Thus, in the physically reasonable limit $\omega_1 \ll \omega_Q$ we see that one satellite of the quadrupolar spectrum can be considered as a single spin-$\frac{1}{2}$ Zeeman-type transition with modified (in fact anisotropic) γ on which one can perform NMR experiments. The last term of (38) is commutative with the rest and can in most cases be disregarded.

$\Delta\omega \sim -\omega_Q$ *and* $\omega_1 \ll \omega_Q$ (*irradiation near high satellite*).

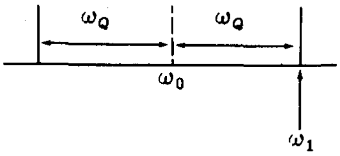

In analogy with the former case we obtain the Hamiltonian in the tilted frame, defined by $U_{z,2}(\frac{1}{2}\pi)$, with $\Delta\omega = -\omega_Q + \delta\omega$,

$$\mathcal{H}_T = -\delta\omega I_{y,3} - (\tfrac{4}{3}\omega_Q - \delta\omega)(I_{z,3} - I_{x,3}) - \sqrt{2}\omega_1(I_{x,1} - I_{y,2}), \tag{39}$$

and with the same arguments, ignoring $\sqrt{2}\omega_1 I_{x,1}$ since $\omega_1 \ll \omega_Q$, we have

$$\mathcal{H}_T = -\delta\omega I_{y,3} + \sqrt{2}\omega_1 I_{y,2} - (\tfrac{4}{3}\omega_Q - \delta\omega)(I_{z,3} - I_{x,3}). \tag{40}$$

This is depicted schematically in Fig. 6.

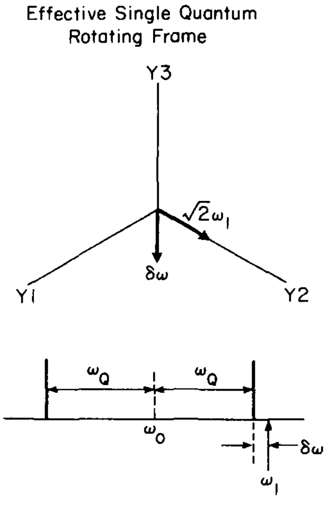

FIG. 6. The same as Fig. 5 except that the irradiation is now near the frequency of the high field quadrupolar satellite. The effective Hamiltonian is now $\mathcal{H} \approx -\delta\omega I_{y,3} + \sqrt{2}\,\omega_1 I_{y,2}$ and the figure shows the y space in which the evolution of the density matrix can be described.

$\Delta\omega \sim 0$ *and* $\omega_1 \ll \omega_Q$.

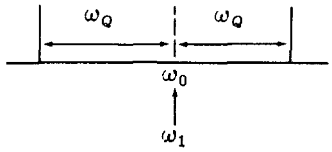

We shall now discuss the Hamiltonian in the rotating frame with an rf irradiation near to the center ($\Delta\omega = \delta\omega$) frequency of the quadrupole spectrum. This of course is the region where we expect to induce double quantum transitions. We shall see how this comes about rigorously. We have

$$\mathcal{H} = -2\delta\omega I_{z,1} - 2\omega_1 I_{x,1} + \tfrac{2}{3}\omega_Q (I_{x,3} - I_{y,3}). \tag{41}$$

To obtain a convenient expression for $\mathcal{H}_T$ we perform the same tilt as was necessary for Eq. (32), transforming to a tilted frame

$$U_{x,2}(\theta) = \exp(i\theta I_{x,2}), \qquad \theta = \tan^{-1}(2\omega_1/\omega_Q),$$

which results in

$$\mathcal{H}_T = -2\delta\omega (I_{z,1}\cos\theta/2 + I_{y,2}\sin\theta/2) + \omega_e I_{x,3} - \tfrac{1}{3}\omega_Q (I_{y,3} - I_{z,3}). \tag{42}$$

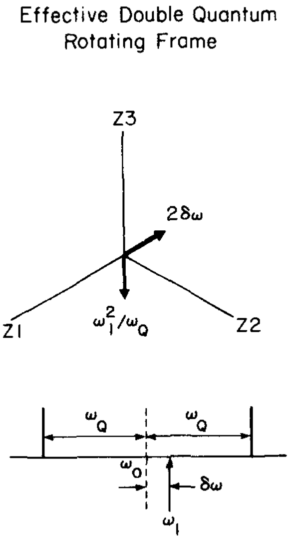

FIG. 7. In this case irradiation is near the unshifted Larmor frequency such that again $\delta\omega_1, \omega_1 \ll \omega_Q$. The effective Hamiltonian in a tilted frame defined in the text is $\mathcal{H} \approx -2\delta\omega I_{z,1} - (\omega_1^2/\omega_Q) I_{z,3}$. Thus the Hamiltonian is that of a fictitious spin-$\frac{1}{2}$ in z space with effective magnetogyric ratio 2γ along $z, 1$ (the effective external field direction) and $(\omega_1/\omega_Q)\gamma$ along $z, 3$ (the effective applied rf field direction). The term double quantum frame arises from the fact that the $I_{z,i}$ operators defining the z frame have matrix elements between the $m = \pm 1$ levels and involve double quantum transitions.

TABLE III. Hamiltonian representations.

$$\Delta\omega = \omega_Q + \delta\omega; \quad \delta\omega,\ \omega_1 \ll \omega_Q$$

$$\mathcal{H}_T = -\delta\omega I_{x,3} - \sqrt{2}\,\omega_1 I_{x,1} - (\tfrac{4}{3}\omega_Q + \delta\omega)(I_{y,3} - I_{z,3})$$

with

$$U = \exp\left(i\,\frac{\pi}{2} I_{z,2}\right)$$

and

$$I_{xT} = \frac{2}{\sqrt{2}}(I_{x,1} - I_{y,2}); \qquad I_{yT} = \frac{2}{\sqrt{2}}(I_{y,1} + I_{x,2})$$

$$\Delta\omega = -\omega_Q + \delta\omega; \quad \delta\omega,\ \omega_1 \ll \omega_Q$$

$$\mathcal{H}_T = -\delta\omega I_{y,3} + \sqrt{2}\,\omega_1 I_{y,2} - (\tfrac{4}{3}\omega_Q - \delta\omega)(I_{z,3} - I_{x,3})$$

with

$$U = \exp\left(i\,\frac{\pi}{2} I_{z,2}\right)$$

and

$$I_{xT} = \frac{2}{\sqrt{2}}(I_{x,1} - I_{y,2}); \qquad I_{yT} = \frac{2}{\sqrt{2}}(I_{y,1} + I_{x,2})$$

$$\Delta\omega = \delta\omega; \quad \delta\omega,\ \omega_1 \ll \omega_Q$$

$$\mathcal{H}_T = -\delta\omega I_{z,1} - \frac{\omega_1^2}{\omega_Q} I_{z,3} + \tfrac{2}{3}\omega_Q (I_{x,3} - I_{y,3})$$

with

$$U = \exp(i\theta I_{x,2}), \qquad \tan\theta = 2\omega_1/\omega_Q$$

and

$$I_{xT} = 2(\cos\theta I_{x,1} - \sin\theta I_{x,3}); \qquad I_{y,T} = 2(\cos\theta/2\, I_{y,1} - \sin\theta/2\, I_{z,2})$$

With the conditions $2\delta\omega\omega_1 \ll \omega_Q^2$ we can neglect the term $2\delta\omega \sin\theta/2\, I_{y,2}$ yielding

$$\mathcal{H}_T \approx -2\delta\omega I_{z,1} - \tfrac{1}{2}(\omega_e - \omega_Q) I_{z,3} + \tfrac{2}{3}\omega_Q (I_{x,3} - I_{y,3}). \tag{43}$$

This shows that even in the case of rf irradiation near to the center frequency we can talk about a fictitious Zeeman interaction in a fictitious z coordinate system. For the case that $\omega_1 \ll \omega_Q$ we can use (35), yielding

$$\mathcal{H}_T \approx -2\delta\omega I_{z,1} - \frac{\omega_1^2}{\omega_Q} I_{z,3} + \tfrac{2}{3}\omega_Q (I_{x,3} - I_{y,3}). \tag{44}$$

This is depicted in Fig. 7 and defines the z frame, or double quantum frame. The effective rf irradiation field along the $z, 3$ axis is ω_1^2/ω_Q and the resonance offset if multiplied by 2, i.e., $2\delta\omega$.

The exact solution for the general case of $\omega_1 \neq 0$, $\Delta\omega \neq 0$, and $\omega_Q \neq 0$ must be calculated by numerical computations, and in Sec. VII we shall discuss some results of those calculations. The main results of this section are summarized in Table III. Also included in the table for future use are the forms of I_x and I_y in the tilted frames, I_{xT} and I_{yT}. After representing possible forms of the Hamiltonian in the rotating frame we now discuss the time behavior of the spin system under the influence of those Hamiltonians and attempt to obtain closed expressions for the signal intensities measured in NMR experiments.

IV. PREPARATION OF SPIN DENSITY MATRIX

We now calculate the evolution of the density matrix during pulses described by the various cases of irradiation in the previous sections. If we define a reduced density matrix appropriate to high temperature, then in the rotating frame

$$\frac{\partial}{\partial t}\rho = -i[\mathcal{H}, \rho].$$

From the equilibrium expression for ρ_0 it is clear that ρ in general can be written as

$$\rho(t) = \sum_{i}^{1,2,3} \sum_{p}^{x,y,z} a_{p,i}(t) I_{p,i} \tag{45}$$

with $a_{p,i}$ calculated from

$$\rho(t) = \exp(-i\mathcal{H}t)\rho(0)\exp(i\mathcal{H}t). \tag{46}$$

Our aim is now to obtain the explicit forms of the last equation for different Hamiltonians derived in the previous section. A variety of specifically interesting cases for NMR spectroscopy will be discussed. The initial signal intensities measured in the corresponding NMR experiments will be calculated.

$\Delta\omega \sim \omega_Q$, $\omega_1 \neq 0$.

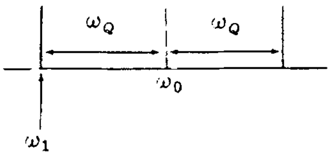

We shall start with the case in which rf irradiation is applied about the resonance of the higher side peak of the quadrupole spectrum, and we shall take as the initial condition for ρ_0 the reduced high temperature equilibrium expression

$$\rho_0 = bI_z$$

with

$$b = \omega_0/kT. \tag{47}$$

We wish now to calculate (46) with $\mathcal{H}$ given in (36). As was shown in (36)–(38), the Hamiltonian can be rewritten in a tilted frame and the result is given in (38) and Table III. We begin by taking the case that $\delta\omega = 0$, i.e., irradiation exactly at one satellite. In this tilted frame ρ_0 becomes

$$\begin{aligned}\rho_{0T} &= U^{\dagger}_{z,2}(\tfrac{1}{2}\pi)\rho_0 U_{z,2}(\tfrac{1}{2}\pi)\\ &= -2bI_{z,3} = bI_{x,3} + b(I_{y,3} - I_{z,3}).\end{aligned} \tag{48}$$

Insertion of ρ_{0T} and $\mathcal{H}_T$ from Table III assuming $\delta\omega = 0$,

$$\mathcal{H}_T = -\sqrt{2}\omega_1 I_{x,1} - \tfrac{4}{3}\omega_Q(I_{y,3} - I_{z,3}),$$

into Eq. (46) yields

$$\begin{aligned}\rho_T(t) &= \exp(-i\mathcal{H}_T t)\rho_{0T}\exp(i\mathcal{H}_T t)\\ &= e^{i\sqrt{2}\omega_1 I_{x,1} t}\, bI_{x,3}\, e^{-i\sqrt{2}\omega_1 I_{x,1} t} + b(I_{y,3} - I_{z,3}), &(49)\\ &= b(I_{x,3}\cos\sqrt{2}\omega_1 t + I_{x,2}\sin\sqrt{2}\omega_1 t) + b(I_{y,3} - I_{z,3}), &(50)\end{aligned}$$

were we used the commutation relations of Table I. It is clear from this result that the density matrix $\rho_T(t)$ can be described in the fictitious x-coordinate system. The last term of $\rho_T(t)$ is not significant for the present experiments because it will not result in an NMR signal. It is crucial of course in many double resonance experiments and constitutes the quadrupolar reservoir. With the result of Eq. (50) we can calculate the signals measured in an NMR experiment, after a pulse in the x direction of duration t, i.e., $\langle I_x(t)\rangle$ and $\langle I_y(t)\rangle$, the expectation values of I_x and I_y in the rotating frame:

$$\begin{aligned}S_x(t) &= \gamma\langle I_x(t)\rangle = \gamma \mathrm{Tr}[\rho(t)I_x] = \gamma\mathrm{Tr}[\rho_T(t)I_{xT}],\\ S_y(t) &= \gamma\langle I_y(t)\rangle = \gamma\mathrm{Tr}[\rho(t)I_y] = \gamma\mathrm{Tr}[\rho_T(t)I_{yT}],\end{aligned} \tag{51}$$

where we used the fact that the trace is independent of the representation of the operators. In our case from Table III,

$$\begin{aligned}I_{xT} &= 2U^{\dagger}_{z,2}(\tfrac{1}{2}\pi)I_{x,1}U_{z,2}(\tfrac{1}{2}\pi) = \sqrt{2}(I_{x,1} - I_{y,2}),\\ I_{yT} &= 2U^{\dagger}_{z,2}(\tfrac{1}{2}\pi)I_{y,1}U_{z,2}(\tfrac{1}{2}\pi) = \sqrt{2}(I_{y,1} + I_{x,2}),\end{aligned} \tag{52}$$

and with Eq. (50) we get the expected result for irradiation in the x direction:

$$S_x(t) = 0,$$

$$S_y(t) = \sqrt{2}\, b\gamma\sin\sqrt{2}\omega_1 t\,\mathrm{Tr}(I^2_{x,2}) = \frac{1}{2\sqrt{2}} S_0\sin\sqrt{2}\omega_1 t, \tag{53}$$

with

$$S_0 = 4Nb\gamma\frac{2^{-1}}{2I+1} = \tfrac{2}{3}N\gamma b,$$

and N is the number of spins in the sample. We want to emphasize here that the effective rotation frequency, due to an irradiation field in the rotating frame, of $\omega_1 = \gamma\mathcal{H}_1$, on one satellite is $\sqrt{2}\omega_1 = \sqrt{2}\gamma\mathcal{H}_1$. This is representative of an effective magnetogyric ratio $\sqrt{2}\gamma$.[1b] The truncation of $\mathcal{H}_T$, by ignoring the term with $I_{y,2}$, is the reason for the fact that the solution of Eq. (53) is not affected by the off resonance satellite of the quadrupolar spectrum at $2\omega_Q$.

The result for irradiation at $\Delta\omega = -\omega_Q$ can be obtained in the same way. Starting from Eq. (40) for $\mathcal{H}_T$ and calculating the values of S_x and S_y gives results analogous to Eq. (53). To complete the description of the NMR signal after a single pulse on one of the satellites of the quadrupole spectrum, we now take into account also $\delta\omega \neq 0$. The Hamiltonian effective for this transition is [Eq. (38) and Table III]

$$\mathcal{H}_T = -\delta\omega I_{x,3} - \sqrt{2}\omega_1 I_{x,1}, \tag{54}$$

where we took $\delta\omega = \Delta\omega - \omega_Q$ and the effective initial condition for ρ in this frame from Eq. (48) is

$$\rho_0 = bI_{x,3}. \tag{55}$$

The signal intensities are proportional to the expectation values of $I_{x,1}$ and $I_{x,2}$:

$$\begin{aligned}S_x(t) &= \sqrt{2}\gamma\mathrm{Tr}[\rho_T(t)I_{x,1}]\\ &= \frac{1}{2\sqrt{2}}S_0\sin\phi\cos\phi(1-\cos\omega_e t),\\ S_y(t) &= \sqrt{2}\gamma\mathrm{Tr}[\rho_T(t)I_{x,2}]\\ &= -\frac{1}{2\sqrt{2}}S_0\cos\phi\sin\omega_e t,\end{aligned} \tag{56}$$

where

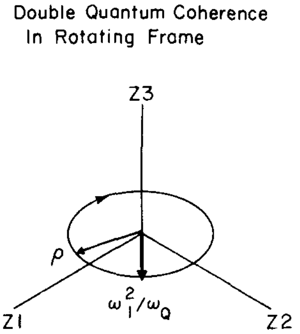

FIG. 8. Preparation of double quantum coherence. The situation is that of Fig. 7 with $\delta\omega = 0$, i.e., irradiation at resonance with $\omega_1 \ll \omega_Q$. The effective Hamiltonian is then $\mathcal{H} \approx -(\omega_1^2/\omega_Q) I_{z,3}$ and its effect on a density matrix starting as $\rho = a_{z,1} I_{z,1}$ (i.e., thermal equilibrium) is shown. The vector ρ nutates as a fictitious spin-$\frac{1}{2}$ about z, 3 at angular frequency ω_1^2/ω_Q. This is analogous to the nutation about x at ω_1 for real spin-$\frac{1}{2}$. In this case the double quantum coherence corresponds to the preparation of a component along z, 2.

$$\omega_s = (\delta\omega^2 + 2\omega_1^2)^{1/2}$$

and

$$\phi = \tan^{-1} \frac{\delta\omega}{\sqrt{2}\omega_1} .$$

This result is in full analogy to a regular Zeeman Hamiltonian as is discussed in Sec. I. The analogous operators for spin-$\frac{1}{2}$ are I_x, I_y, and I_z for $I_{x,1}$, $I_{x,2}$, and $I_{x,3}$, respectively.

$\Delta\omega \sim 0,\ \omega_1 \ll \omega_Q.$

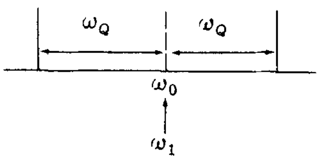

The discussion of rf irradiation at the center frequency of the spectrum is interesting from the point of view of double quantum effects in our three level system. In this section we shall discuss the creation of coherence of the double quantum transition. In this case, according to Table III, the Hamiltonian in the frame tilted by $U_{x,2}(\theta)$ with $\theta = \tan^{-1}(2\omega_1/\omega_Q)$ and $4\delta\omega_1 \ll \omega_Q^2$ is

$$\mathcal{H}_T = -2\delta\omega I_{z,1} - \tfrac{1}{2}[(\omega_Q^2 + 4\omega_1^2)^{1/2} - \omega_Q] I_{z,3} + \tfrac{2}{3}\omega_Q (I_{x,3} - I_{y,3}). \tag{57}$$

To evaluate Eq. (46) for this case we transform ρ_0 in Eq. (47) according to $U_{x,2}(\theta)$:

$$\begin{aligned}\rho_{0T} &= 2b \exp(-i\theta I_{x,2}) I_{z,1} \exp(i\theta I_{x,2}) \\ &= 2b (I_{z,1} \cos\theta/2 + I_{y,2} \sin\theta/2).\end{aligned} \tag{58}$$

We calculate $\rho_T(t)$ by inserting Eqs. (57) and (58) in Eq. (46) with $\delta\omega = 0$ (i.e., we assume $\omega_e - \omega_\alpha \gg \delta\omega$):

$$\begin{aligned}\rho_T(t) &= \exp(-i\mathcal{H}_T t)\, \rho_{0T} \exp(+i\mathcal{H}_T t) \\ &= 2b\, e^{i(1/2)(\omega_e - \omega_Q) I_{z,3} t}\, I_{z,1}\, e^{-i(1/2)(\omega_e - \omega_Q) I_{z,3} t} \cos\theta/2 + 2b\, e^{+i(1/2)(\omega_e + \omega_Q) I_{y,3} t}\, I_{y,2}\, e^{-i(1/2)(\omega_e + \omega_Q) I_{y,3} t} \sin\theta/2 \\ &= 2b[I_{z,1} \cos\tfrac{1}{2}(\omega_e - \omega_Q)t - I_{z,2} \sin\tfrac{1}{2}(\omega_e - \omega_Q)t] \cos\theta/2 + 2b[I_{y,2} \cos\tfrac{1}{2}(\omega_e + \omega_Q)t + I_{y,1} \sin\tfrac{1}{2}(\omega_e + \omega_Q)t] \sin\theta/2,\end{aligned} \tag{59}$$

where we recall [Eq. (33)] that

$$\omega_e = (4\omega_1^2 + \omega_Q^2)^{1/2} .$$

The calculated behavior of $\rho_T(t)$ becomes for $\omega_1 \ll \omega_Q$ [Eq. (35)]

$$\rho_T(t) \approx 2b \left(I_{z,1} \cos \frac{\omega_1^2}{\omega_Q} t - I_{z,2} \sin \frac{\omega_1^2}{\omega_Q} t \right). \tag{60}$$

The second term in Eq. (60) *represents the coherence of the double quantum transition, because it has matrix elements between the* $|+1\rangle$ *and* $|-1\rangle$ *eigenstates of* I_z *and it behaves as the coherent superposition of these states.* For the case $\omega_1 \ll \omega_Q$ we can again talk effectively about a fictitious Zeeman-type Hamiltonian on the transition $|+1\rangle - |-1\rangle$. The preparation of the density matrix in this case is depicted schematically in Fig. 8 for $\delta\omega = 0$. We refer to such a pulse with $\omega_1 \ll \omega_Q$ and $4\delta\omega\omega_1 \ll \omega_Q^2$ as a double quantum pulse. The effective Hamiltonian in this case is obtained from (35) and (57):

$$\mathcal{H}_T = -2\delta\omega I_{z,1} - \frac{\omega_1^2}{\omega_Q} I_{z,3}. \tag{61}$$

The effective magnetogyric ratio is $(\omega_1/\omega_Q)\gamma$ and the off resonance term is 2 times the offset frequency. The rotation frequency of spins around $I_{z,3}$ is ω_1^2/ω_Q and was already observed by Hatanaka *et al.*[3]

The observables S_x and S_y subsequent to preparation by a double quantum pulse can be calculated from Eqs. (51) and (59):

$$\begin{aligned}I_{x,T} &= 2U_{x,2}^\dagger(\theta) I_{x,1} U_{x,2}(\theta) = 2(I_{x,1} \cos\theta - I_{x,3} \sin\theta), \\ I_{y,T} &= 2U_{x,2}^\dagger(\theta) I_{y,1} U_{x,2}(\theta) = 2(I_{y,1} \cos\tfrac{1}{2}\theta - I_{z,2} \sin\tfrac{1}{2}\theta),\end{aligned} \tag{62}$$

and become

$$\begin{aligned}S_x &= \gamma \operatorname{Tr}[\rho_T(t) I_{xT}] = 0, \\ S_y &= \gamma \operatorname{Tr}[\rho_T(t) I_{yT}] \\ &= \tfrac{1}{2}\gamma S_0 \sin\theta [\sin\tfrac{1}{2}(\omega_e - \omega_Q)t + \sin\tfrac{1}{2}(\omega_e + \omega_Q)t] \\ &\approx 0 \text{ since } \omega_1 \ll \omega_Q \text{ giving } \sin\theta \approx 0.\end{aligned} \tag{63}$$

Thus, after such a pulse there is essentially no observable signal, i.e., the double quantum coherent state does not evolve with an observable signal. Since $I_{z,2}$ and $I_{z,3}$ are related to the coherence of ± 1 transitions, we define the double quantum coherence in the case that $I_{z,2}$ is prepared:

$$Q(t)=2\gamma\,\mathrm{Tr}\,[\rho(t)\,I_{z,2}]=2\gamma\,\mathrm{Tr}\,[\rho_T(t)\,I_{z,2T}], \qquad (64)$$

or similarily with $I_{z,3}$ or a combination of $I_{z,2}$ and $I_{z,3}$. $Q(t)$, as mentioned above, is not an observable in an NMR experiment. It can be calculated in our case using

$$I_{z,2T}=U^\dagger_{x,2}(\theta)\,I_{z,2}\,U_{x,2}(\theta)=I_{z,2}\cos\tfrac{1}{2}\theta+I_{y,1}\sin\tfrac{1}{2}\theta, \qquad (65)$$

giving

$$Q(t)=-S_0\,[\cos^2\tfrac{1}{2}\theta\,\sin\tfrac{1}{2}(\omega_e-\omega_Q)t \\ -\sin^2\tfrac{1}{2}\theta\,\sin\tfrac{1}{2}(\omega_e+\omega_Q)t\,]. \qquad (66)$$

The coherence $Q(t)$ is maximum in the case of $\omega_1 \ll \omega_Q$ for

$$\tfrac{1}{2}(\omega_e-\omega_Q)\,t\approx(\omega_1^2/\omega_Q)t=\tfrac{1}{2}\pi. \qquad (67)$$

Thus the $\frac{1}{2}\pi$ condition for a double quantum pulse with $\omega_1 \ll \omega_Q$ is given by $(\omega_1^2/\omega_Q)\,t=\frac{1}{2}\pi$. This is a $\frac{1}{2}\pi$ double quantum pulse.

The preparation of the density matrix in the rotating frame for the general case during rf irradiation with $\delta\omega \neq 0$ is complicated and is best calculated with the help of a high speed computer. In the next section, we shall discuss the evolution of the spin system without rf irradiation after the density matrix has been prepared in nonequilibrium form. The signal intensities measured after rf pulses will be discussed and the Fourier transforms of different FID signals will be given.

V. EVOLUTION AND SIGNALS

In this section we give the equations for the density matrix of the spin system in terms of our nine operators for the case that no rf irradiation is applied to the system. We assume the system to be in a nonequilibrium state after some preparation and ask how it evolves with time. This corresponds to the behavior of the spin system after an excitation pulse. We ignore for simplicity all relaxation effects.

The evolution of the spin density matrix under the influence of the main Hamiltonian without rf irradiation,

$$\mathcal{H}=-2\Delta\omega I_{z,1}+\tfrac{2}{3}\omega_Q(I_{x,3}-I_{y,3}),$$

is calculated by inserting this Hamiltonian in the solution for $\rho(t)$ in Eq. (46). The signal intensities are then proportional to the expectation values of I_x and I_y. We shall therefore first derive the time behavior of an arbitrary $\rho(0)$ due to $\mathcal{H}$ and shall show which of the coefficients of $\rho(0)$,

$$\rho(0)=\sum_{ip} a_{p,i}(0)\,I_{p,i}, \qquad (68)$$

are subsequently detectable. A straightforward calculation gives for the coefficients $a_{p,i}(t)$, with the assumption that $a_{p,3}(0)=0$, $p=x,\ y,\ z$,

$$\begin{aligned}
a_{x,1}(t)&=\tfrac{1}{2}[a_{x,1}(0)+a_{y,2}(0)]\cos(\omega_Q-\Delta\omega)t-\tfrac{1}{2}[a_{x,2}(0)+a_{y,1}(0)]\sin(\omega_Q-\Delta\omega)t\\
&\quad-\tfrac{1}{2}[a_{y,1}(0)-a_{x,2}(0)]\sin(-\omega_Q-\Delta\omega)t-\tfrac{1}{2}[a_{y,2}(0)-a_{x,1}(0)]\cos(-\omega_Q-\Delta\omega)t,\\
a_{x,2}(t)&=\tfrac{1}{2}[a_{x,2}(0)+a_{y,1}(0)]\cos(\omega_Q-\Delta\omega)t+\tfrac{1}{2}[a_{x,1}(0)+a_{y,2}(0)]\sin(\omega_Q-\Delta\omega)t\\
&\quad-\tfrac{1}{2}[a_{y,1}(0)-a_{x,2}(0)]\cos(-\omega_Q-\Delta\omega)t+\tfrac{1}{2}[a_{y,2}(0)-a_{x,1}(0)]\sin(-\omega_Q-\Delta\omega)t,\\
a_{y,1}(t)&=\tfrac{1}{2}[a_{y,1}(0)-a_{x,2}(0)]\cos(-\omega_Q-\Delta\omega)t-\tfrac{1}{2}[a_{y,2}(0)-a_{x,1}(0)]\sin(-\omega_Q-\Delta\omega)t\\
&\quad+\tfrac{1}{2}[a_{x,1}(0)+a_{y,2}(0)]\sin(\omega_Q-\Delta\omega)t+\tfrac{1}{2}[a_{x,2}(0)-a_{y,1}(0)]\cos(\omega_Q-\Delta\omega)t,\\
a_{y,2}(t)&=\tfrac{1}{2}[a_{y,2}(0)-a_{x,1}(0)]\cos(-\omega_Q-\Delta\omega)t+\tfrac{1}{2}[a_{y,1}(0)-a_{x,2}(0)]\sin(-\omega_Q-\Delta\omega)t\\
&\quad+\tfrac{1}{2}[a_{x,1}(0)+a_{y,2}(0)]\cos(\omega_Q-\Delta\omega)t-\tfrac{1}{2}[a_{x,2}(0)+a_{y,1}(0)]\sin(\omega_Q-\Delta\omega)t,\\
a_{z,1}(t)&=a_{z,1}(0),\\
a_{z,2}(t)&=a_{z,2}(0)\cos 2\Delta\omega t,\\
a_{z,3}(t)&=-a_{z,2}(0)\sin 2\Delta\omega t,\\
a_{x,3}(t)&=-a_{y,3}(t)=0.
\end{aligned} \qquad (69)$$

For the special case that $\Delta\omega=0$, we get

$$\begin{aligned}
a_{x,1}(t)&=a_{x,1}(0)\cos\omega_Q t-a_{x,2}(0)\sin\omega_Q t,\\
a_{x,2}(t)&=a_{x,1}(0)\sin\omega_Q t+a_{x,2}(0)\cos\omega_Q t,\\
a_{y,1}(t)&=a_{y,1}(0)\cos\omega_Q t+a_{y,2}(0)\sin\omega_Q t,\\
a_{y,2}(t)&=-a_{y,1}(0)\sin\omega_Q t+a_{y,2}(0)\cos\omega_Q t.
\end{aligned} \qquad (70)$$

These expressions are calculated by the following procedure:

$$a_{p,i}(t)=\mathrm{Tr}\,[\rho_T(t)\,U^\dagger_{z,2}(\tfrac{1}{2}\pi)\,I_{p,i}\,U_{z,2}(\tfrac{1}{2}\pi)]\ , \qquad (71)$$

with

$$\rho_T(t)=\sum_{p,i} a_{p,i}(0)\exp(-i\mathcal{H}_T t) \\ \times\ U^\dagger_{z,2}(\tfrac{1}{2}\pi)\,I_{p,i}\,U_{z,2}(\tfrac{1}{2}\pi)\exp(+i\mathcal{H}_T t) \qquad (72)$$

and

$$\mathcal{H}_T=U^\dagger_{z,2}(\tfrac{1}{2}\pi)\,\mathcal{H}\,U_{z,2}(\tfrac{1}{2}\pi). \qquad (73)$$

The result for the FID signal can now be calculated:

$$S_x=\gamma\,\mathrm{Tr}\,[\rho(t)\,I_x]=a_{x,1}(t)\,\psi(t),$$

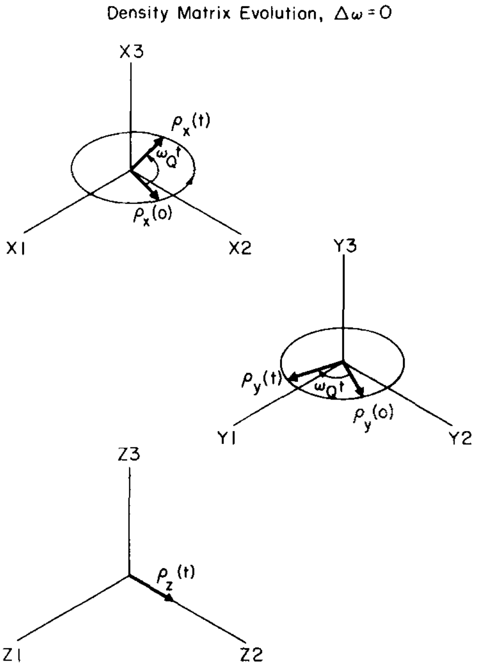

FIG. 9. Schematic description of the evolution of the spin density matrix under the influence of the quadrupolar Hamiltonian $\mathcal{H}_Q = \frac{2}{3}\omega_Q(I_{x,3} - I_{y,3})$ on resonance, (i.e., $\Delta\omega = 0$). The density matrix can be expanded as $\rho = \rho_x + \rho_y + \rho_z$, where $\rho_p = \sum_i a_{p,i} I_{p,i}$. The figure demonstrates that in the case that all $a_{p,3}(0) = 0$, ρ_x rotates in the 1–2 plane in x space at frequency ω_Q, ρ_y in y space, and ρ_z stays constant in z space.

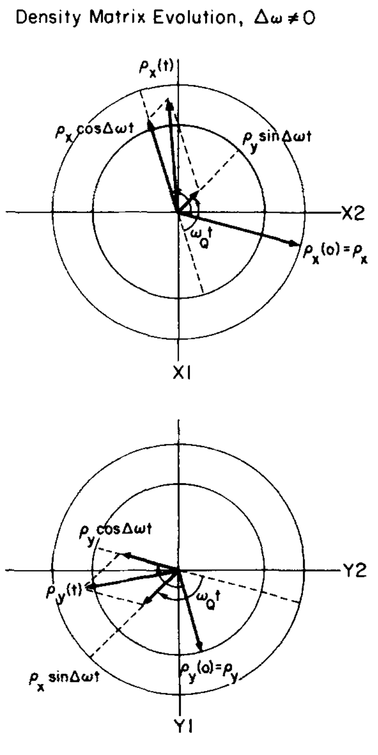

FIG. 10. Same as Fig. 9 for the case that $\Delta\omega \neq 0$. In this case the x and y frames are coupled together. The figure shows the evolution of the x and y components of the density matrix $\rho_x(0) = a_{x,1}I_{x,1} + a_{x,2}I_{x,2}$ and $\rho_y(0) = a_{y,1}I_{y,1} + a_{y,2}I_{y,2}$ under the influence of the quadrupole and resonance offset Hamiltonians.

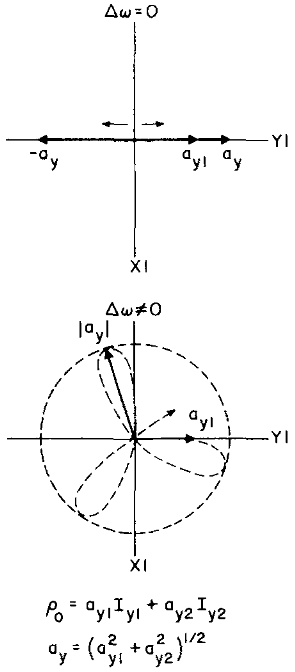

FIG. 11. The observables in an *nmr* experiment are $\langle I_{x,1}\rangle$ and $\langle I_{y,1}\rangle$. The evolution of the coefficients of these components of the density matrix, $a_{x,1}$ and $a_{y,1}$ under the influence of the quadrupolar Hamiltonian for $\Delta\omega = 0$ and the quadrupolar plus resonance offset Hamiltonians for $\Delta\omega \neq 0$, are shown for the case that the initial density matrix is given by $a_{y,1}I_{y,1} + a_{y,2}I_{y,2}$.

$$S_y = \gamma \operatorname{Tr}[\rho(t) I_y] = a_{y,1}(t)\psi(t), \tag{74}$$

where $\psi(t)$ is a decaying function with a decay time T_2 and $\psi(0) = \frac{1}{3}\gamma N = S_0$. The coherence of the double quantum transition is defined as

$$Q(t) = a_{z,2}(t)\psi(t). \tag{75}$$

A schematic representation of the results of Eqs. (69) and (70) is shown in Figs. 9 and 10. The x- and y-components of the a_p vectors are defined by the coefficients of

$$\rho_y(t) = \sum_i a_{y,i}(t) I_{y,i},$$

$$\rho_x(t) = \sum_i a_{x,i}(t) I_{x,i}, \tag{76}$$

respectively, i.e., a_p is the vector defined by the components $a_{p,i}$. The time evolution of the z vector defined by the coefficients of

$$\rho_z(t) = \sum_i a_z(t) I_{z,i} \tag{77}$$

is also shown. From the results of Eqs. (69)–(75) and of Fig. 9, we see that in the case of $\Delta\omega = 0$ the signal is linearly polarized. This is also demonstrated in Fig. 11 for the case $\rho_0 = a_{y,1}I_{y,1} + a_{y,2}I_{y,2}$. We find in this case for the detected signals

$$S_x = 0,$$

$$S_y = (a_{y,1}\cos\omega_Q t + a_{y,2}\sin\omega_Q t)\,\psi(t)$$

$$= \gamma a_y \cos(\omega_Q t - \phi)\,\psi(t), \tag{78}$$

where $a_y = (a_{y,1} + a_{y,2})^{1/2}$ and $\phi = \tan^{-1}(a_{y,1}/a_{y,2})$.

The results for $\Delta\omega \neq 0$ with the same initial condition is given by

$$S_x = a_y \cos(\omega_Q t - \phi)\sin\Delta\omega t\psi(t),$$

TABLE IV. Effect of rf irradiation on spin-$\frac{1}{2}$ operators.

$$\exp(-i\mathcal{H}t)I_{p,i}\exp(i\mathcal{H}t)=\sum_{q,j}(p,i;q,j)I_{q,j}$$

$$(x,1;x,1)=\cos^2\theta\cos\omega_e t+\sin^2\theta$$
$$(x,1;x,2)=\cos\theta\sin\omega_e t$$
$$(x,1;x,3)=\cos\theta\sin\theta(\cos\omega_e t-1)$$

$$(x,2;x,1)=-\cos\theta\sin\omega_e t$$
$$(x,2;x,2)=\cos\omega_e t$$
$$(x,2;x,3)=-\sin\theta\sin\omega_e t$$

$$(y,1;y,1)=\cos^2\theta/2\cos\tfrac{1}{2}(\omega_e+\omega_Q)t+\sin^2\theta/2\cos\tfrac{1}{2}(\omega_e-\omega_Q)t$$
$$(y,1;y,2)=-\cos^2\theta/2\sin\tfrac{1}{2}(\omega_e+\omega_Q)t+\sin^2\theta/2\sin\tfrac{1}{2}(\omega_e-\omega_Q)t$$
$$(y,1;z,1)=-\cos\theta/2\sin\theta/2[\sin\tfrac{1}{2}(\omega_e+\omega_Q)t+\sin\tfrac{1}{2}(\omega_e-\omega_Q)t]$$
$$(y,1;z,2)=\cos\theta/2\sin\theta/2[\cos\tfrac{1}{2}(\omega_e+\omega_Q)t-\cos\tfrac{1}{2}(\omega_e-\omega_Q)t]$$

$$(y,2;y,1)=\cos^2\theta/2\sin\tfrac{1}{2}(\omega_e+\omega_Q)t-\sin^2\theta/2\sin\tfrac{1}{2}(\omega_e-\omega_Q)t$$
$$(y,2;y,2)=\cos^2\theta/2\cos\tfrac{1}{2}(\omega_e+\omega_Q)t+\sin^2\theta/2\cos\tfrac{1}{2}(\omega_e-\omega_Q)t$$
$$(y,2;z,1)=\cos\theta/2\sin\theta/2[\cos\tfrac{1}{2}(\omega_e+\omega_Q)t-\cos\tfrac{1}{2}(\omega_e-\omega_Q)t]$$
$$(y,2;z,2)=\cos\theta/2\sin\theta/2[\sin\tfrac{1}{2}(\omega_e+\omega_Q)t+\sin\tfrac{1}{2}(\omega_e-\omega_Q)t]$$

$$(z,1,y,1)=\cos\theta/2\sin\theta/2[\sin\tfrac{1}{2}(\omega_e+\omega_Q)t+\sin\tfrac{1}{2}(\omega_e-\omega_Q)t]$$
$$(z,1,y,2)=\cos\theta/2\sin\theta/2[\cos\tfrac{1}{2}(\omega_e+\omega_Q)t-\cos\tfrac{1}{2}(\omega_e-\omega_Q)t]$$
$$(z,1;z,1)=\sin^2\theta/2\cos\tfrac{1}{2}(\omega_e+\omega_Q)t+\cos^2\theta/2\cos\tfrac{1}{2}(\omega_e-\omega_Q)t$$
$$(z,1;z,2)=\sin^2\theta/2\sin\tfrac{1}{2}(\omega_e+\omega_Q)t-\cos^2\theta/2\sin\tfrac{1}{2}(\omega_e-\omega_Q)t$$

$$(z,2;y,1)=\cos\theta/2\sin\theta/2[\cos\tfrac{1}{2}(\omega_e+\omega_Q)t-\cos\tfrac{1}{2}(\omega_e-\omega_Q)t]$$
$$(z,2;y,2)=-\cos\theta/2\sin\theta/2[\sin\tfrac{1}{2}(\omega_e+\omega_Q)t+\sin\tfrac{1}{2}(\omega_e-\omega_Q)t]$$
$$(z,2;z,1)=-\sin^2\theta/2\sin\tfrac{1}{2}(\omega_e+\omega_Q)t+\cos^2\theta/2\sin\tfrac{1}{2}(\omega_e-\omega_Q)t$$
$$(z,2;z,2)=\sin^2\theta/2\cos\tfrac{1}{2}(\omega_e+\omega_Q)t+\cos^2\theta/2\cos\tfrac{1}{2}(\omega_e-\omega_Q)t$$

with

$$\mathcal{H}=-2\omega_1 I_{x,1}+\tfrac{2}{3}\omega_Q(I_{x,3}-I_{y,3})$$

and

$$\omega_e=(4\omega_1^2+\omega_Q^2)^{1/2}$$
$$\theta=\tan^{-1}(2\omega_1/\omega_Q)$$

$$S_y=a_y\cos(\omega_Q t-\phi)\cos\Delta\omega t\psi(t). \qquad (79)$$

For completeness we give in Table IV the results of $\rho(0)$ after a resonant ($\Delta\omega=0$) pulse of t seconds and of ω_1 strength in the x direction for different initial density matrices just before the pulse.

The evolution of $a_{z,2}(t)$ and $a_{z,3}(t)$ in Eqs. (69) is particularly interesting. Although they are not directly detectable as mentioned previously, the time dependence does not contain ω_Q, i.e., they do not exhibit any quadrupolar interaction. Thus if their decay could be monitored, they would yield a high resolution NMR spectrum. This indeed is the basis for the approach we have termed *Fourier transform double quantum NMR.*

To observe a pure double quantum decay, the system must be prepared so that

$$\rho(0)=a_{z,2}I_{z,2}+a_{z,3}I_{z,3}.$$

After time t the double quantum coherence which has evolved only with $2\Delta\omega$ must be detected by an additional pulse or set of pulses. In the next section this is discussed in detail both for the ideal double quantum case $\omega_1\ll\omega_Q$ and for the more practical case of general ω_1.

VI. DOUBLE QUANTUM COHERENCE

In this section, examples of different pulse sequences will be discussed. We shall be interested in the efficiency of formation of $I_{z,2}$, double quantum coherence, and its detection by pulses since it is not directly detectable as an NMR signal. First the effect of a single pulse on the spin system will be described and the physical observables will be derived. In all the examples discussed below, we take $\Delta\omega=0$ during the pulses, i.e., we assume $\omega_1\gg\Delta\omega$ and $\omega_1^2/\omega_Q\gg\Delta\omega$. When there is no rf irradiation we take account of $\Delta\omega$.

A. One pulse (Fig. 12)

Applying a short rf pulse on our system results in a new density matrix after this pulse given in Table IV. These results are simplified in Table V for the special cases of very strong ($\omega_1\gg\omega_Q$) and very weak ($\omega_1\ll\omega_Q$) irradiation. In the former case we expect pure rotations, i.e., normal single quantum behavior, and in the second one expect double quantum effects. The results of this table are calculated from Eq. (46) with $\mathcal{H}$ as given in Table III:

$$\omega_1\ll\omega_Q:\ \mathcal{H}\approx-(\omega_1^2/\omega_Q)I_{z,3}+\tfrac{2}{3}\omega_Q(I_{x,3}-I_{y,3}),$$

and

$$\omega_1\gg\omega_Q:\ \mathcal{H}\approx-2\omega_1 I_{x,1}. \qquad (80)$$

From the results of Table V we can answer the question of which pulse we need to apply in order to obtain a detectable signal or to create double quantum coherence. From the discussion of the previous section we know that the only coefficients of $\rho(t)$ which give rise to detectable signals during evolution are $a_{x,1}$, $a_{x,2}$, $a_{y,1}$, and $a_{y,2}$. These coefficients can be created for example from $I_{z,1}$ and $I_{z,2}$ by $\omega_1\gg\omega_Q$, while for $\omega_1\ll\omega_Q$ the double quantum coherence coefficient $a_{z,2}$ is obtained. For comparison between the exact solutions of Table IV and the approximated solutions of Table V we have plotted in Figs. 13 and 14 the coefficients of $I_{z,2}$ and $I_{y,1}$ as functions of the length of an x pulse with $\nu_1=20$ kHz and $\nu_Q=60$ kHz for $\rho_i=I_{z,1}$. For pure double

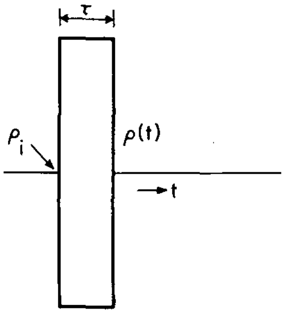

FIG. 12. Single rf pulse of duration τ operates on the density matrix ρ_i and transforms it to ρ which evolves as $\rho(t)$. τ in this figure corresponds to t in Table IV.

TABLE V. Form of density matrix after strong (single quantum) and weak (double quantum) pulse on different initial density matrices.

	Single quantum $\omega_1 \gg \omega_Q$, $\Delta\omega = 0$	Double quantum $\omega_1 \ll \omega_Q$, $\Delta\omega = 0$
ρ_i	p Pulse	x Pulse
$I_{p,1}$	$I_{p,1}$	
$I_{p,2}$	$I_{p,2}\cos 2\omega_1 t - I_{p,3}\sin 2\omega_1 t$	
$I_{p,3}$	$I_{p,3}\cos 2\omega_1 t + I_{p,2}\sin 2\omega_1 t$	
$I_{q,1}$	$I_{q,1}\cos\omega_1 t - I_{r,1}\sin\omega_1 t$	
$I_{q,2}$	$I_{q,2}\cos\omega_1 t + I_{r,2}\sin\omega_1 t$	
$I_{q,3}$	$-\frac{1}{2}(I_{p,3}\cos 2\omega_1 t + I_{p,2}\sin 2\omega_1 t) + \frac{1}{2}(I_{q,3} - I_{r,3})$	
$I_{r,1}$	$I_{r,1}\cos\omega_1 t + I_{q,1}\sin\omega_1 t$	$I_{z,1}\cos(\omega_1^2/\omega_Q)t - I_{z,2}\sin(\omega_1^2/\omega_Q)t$
$I_{r,2}$	$I_{r,2}\cos\omega_1 t - I_{q,2}\sin\omega_1 t$	$I_{z,2}\cos(\omega_1^2/\omega_Q)t + I_{z,1}\sin(\omega_1^2/\omega_Q)t$
$I_{r,3}$	$-\frac{1}{2}(I_{p,3}\cos 2\omega_1 t + I_{p,2}\sin 2\omega_1 t) - \frac{1}{2}(I_{q,3} - I_{r,3})$	$I_{z,3}$
	$p, q, r = x, y, z$ or y, z, x	$p, q, r = x, y, z$

quantum behavior $\omega_1 \ll \omega_Q$, we expect from Table V $a_{z,2} = -\sin(\omega_1^2/\omega_Q)t$.

The results of the coefficient of $I_{z,1}$ (Fig. 15) and $I_{z,2}$ (Fig. 16) are shown as functions of ν_Q for a fixed pulse time $\tau = 56$ μsec and $\tau = 28\mu$sec, respectively. *This is to indicate the degree to which we can create double quantum coherence, $I_{z,2}$ over a continuous range of ω_Q.* The approximated results are in reasonable agreement with the exact calculations for $\omega_Q > 2.5\,\omega_1$.

To illustrate the case where ω_1 is larger than ω_Q, we take $\nu_1 = 60$ kHz and $\nu_Q = 20$ kHz. The approximated results and the exact calculation are compared in Fig. 17 for the coefficient of $I_{y,1}$ as functions of the pulse length, with $\rho_i = I_{z,1}$. We see that for long pulses the approximated solution is out of phase with the exact calculation. This comes from the fact that even in this case ($\nu_1 > \nu_Q$) some $a_{z,2}$ is formed. In Fig. 18 we show the $I_{z,2}$ coefficient as a function of ν_Q for a constant pulse length of 16μsec. We see that at $\nu_Q = 20$ the coefficient of $I_{z,2}$ is $a_{z,2} = 0.84$. In Fig. 19 we also show an experimental result on a single crystal of deuterated oxalic acid dihydrate. In this experiment the value of $a_{z,1}$ after a single pulse probes how much $I_{z,1}$ is left. The $a_{z,1}$ value is detected by a second pulse, which is applied at time T_2 following the first pulse. The signal after this second pulse is then proportional to $a_{z,1}$ and is plotted as a function of the length of the first pulse. The experimental values are compared with the calculated $a_{z,1}$ values for the experimental parameters $\nu_1 = 26$ kHz and $\nu_Q = 16$ kHz from Eq. (69).

In Table VI we summarize the effects of pulses of particular length corresponding to a 90° rotation for

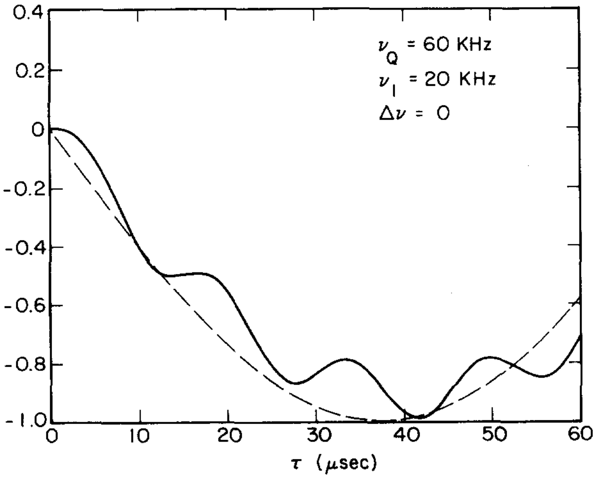

FIG. 13. Theoretical calculation of the effect of a single pulse with $\nu_1 = 20$ kHz at resonance to the density matrix $\rho_0 = I_{z,1}$. The solid line is the exact (computer generated) value of the double quantum coherence coefficient $a_{z,2}$ as a function of the pulse length. The dashed line shows behavior expected for pure double quantum transitions, i.e., $a_{z,2} = -\sin(\omega_1^2/\omega_Q)\tau$. The discrepancy arises from the fact that ω_1/ω_Q is not zero, i.e., single quantum transitions are also induced.

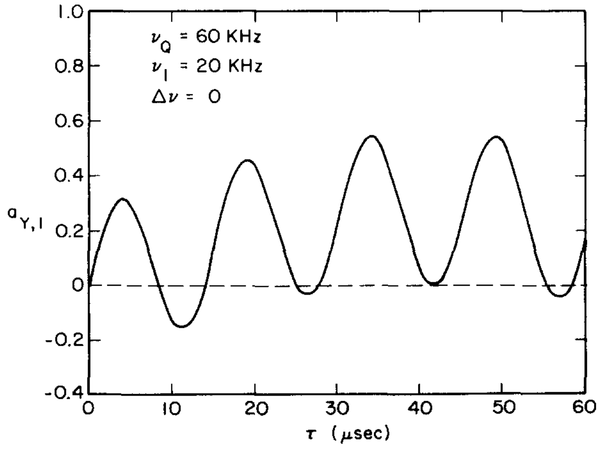

FIG. 14. The same parameters as Fig. 13 except that the observable y signal, $a_{y,1}$, is presented, solid line (exact calculations). For pure double quantum transitions we should have $a_{y,1} = 0$ as indicated by the dashed line.

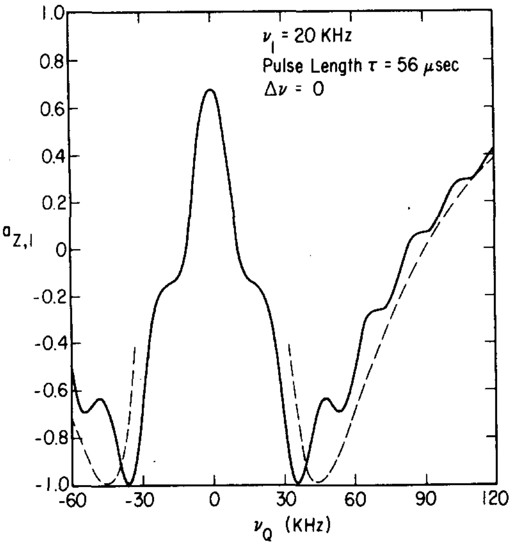

FIG. 15. Theoretical calculation of the remaining z magnetization $a_{z,1}$ for an rf pulse of intensity $\nu_1 = 20$ kHz and duration 56 μsec applied to the equilibrium density matrix $I_{z,1}$ as a function of quadrupole splitting $\nu_Q = \omega_Q/2\pi$. The solid line is an exact calculation and the dashed line indicates the expected behavior for pure double quantum behavior $a_{z,1} = \cos(\omega_1^2/\omega_Q)\tau$. For large ω_Q the agreement becomes better as ω_1/ω_Q gets smaller, while for small ω_Q the double quantum expression is of course not valid.

the single quantum case $\omega_1 \gg \omega_Q$ where the effective rotary frequencies are ω_1 or $2\omega_1$ and for the double quantum case $\omega_1 \ll \omega_Q$ where the effective frequency is ω_1^2/ω_Q.

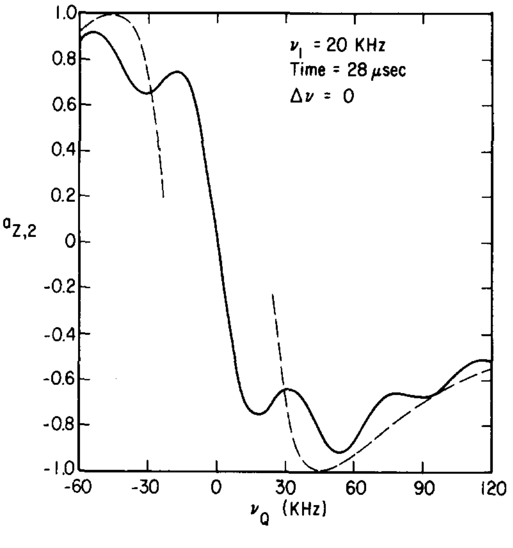

FIG. 16. Preparation of double quantum coherence with a single pulse. An rf pulse of intensity $\nu_1 = 20$ kHz and duration 28 μsec is applied to $\rho_0 = I_{z,1}$ and the calculated values of $a_{z,2}$ are shown as a function of ω_Q. The solid line is an exact calculation showing the distortion in preparation of double quantum coherence when we have a range of ω_Q values as in a polycrystalline sample. The dashed line is that expected for pure double quantum behavior $a_{z,2} = -\sin(\omega_1^2/\omega_Q)t$ which becomes more valid for small ω_1/ω_Q.

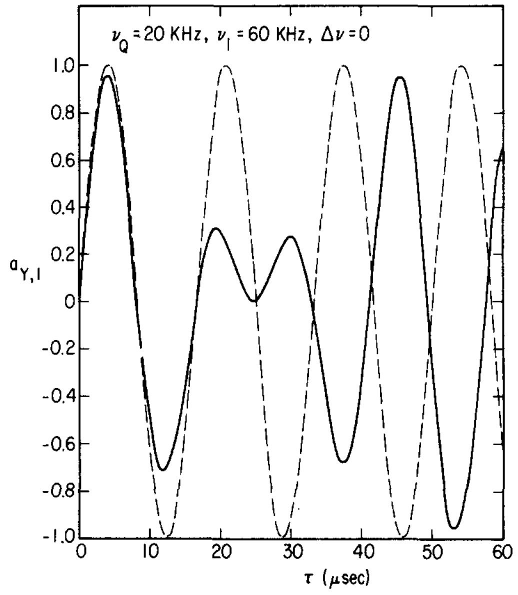

FIG. 17. Effect of intense rf pulse on the density matrix $I_{z,1}$. The coefficient of the observable signal is plotted from an exact calculation (solid line) and for pure single quantum behavior $\sin\omega_1 t$ (dashed line).

B. Two pulses (Fig. 20)

In this paragraph we shall discuss the effects of three different two-pulse sequences which then will be used later for the detection of double quantum coherence in single crystals and powders.

1. *Two weak pulses*

The application of two x pulses of equal length and strength Fig. 20(a) is used for the storage of $a_{z,2}$. What we mean by this is that after a single weak pulse (Table V) on $\rho_i = I_{z,1}$ the density matrix contains a coefficient $a_{z,2} \neq 0$. This coefficient of $I_{z,2}$ after the pulse can then

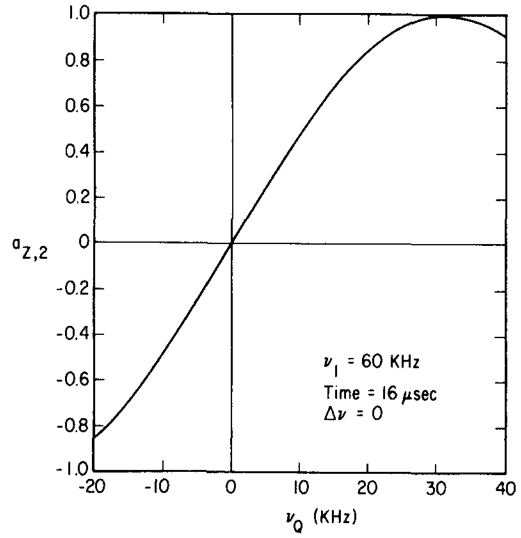

FIG. 18. Calculation of double quantum coherence for intense pulse of duration 16 μsec operating on $I_{z,1}$. This shows that even for large ν_1 we can create double quantum coherence for particular ω_Q's.

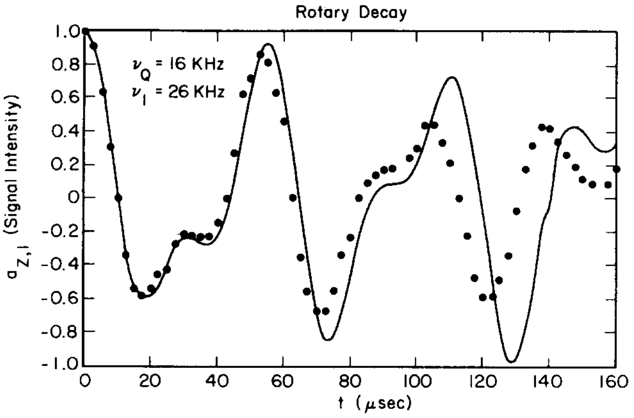

FIG. 19. Rotary free induction decay for pulse of intensity $\nu_1 = 26$ MHz followed by intense pulse to monitor remaining $a_{z,1}$. The solid line is calculated from Eq. (69) and the circles are experimental points from a single crystal of deuterated oxalic acid dihydrate.

evolve for a time τ after which it can be brought back to a coefficient of $I_{z,1}$ by an additional weak pulse. It will be shown later that this can be of importance for the detection of the time behavior of $a_{z,2}$, the coherence. With the assumptions $\omega_1 \ll \omega_Q$ and $\Delta\omega \ll \omega_Q$ the results for the density matrix in this case are

TABLE VI. Effective $\frac{1}{2}\pi$ pulses.

ρ_i	$\omega_1 \gg \omega_Q$ $\omega_1 t$	ρ_f	ρ_i	$\omega_1 \ll \omega_Q$ $\frac{\omega_1^2}{\omega_Q} t$	ρ_f
	x Pulse			x Pulse	
$I_{x,1}$	$\cdots$	$I_{x,1}$	$I_{z,1}$	$\pi/2$	$-I_{z,2}$
$I_{x,2}$	$\pi/4$	$-I_{x,3}$	$I_{z,2}$	$\pi/2$	$I_{z,1}$
$I_{x,3}$	$\pi/4$	$I_{x,2}$	$I_{z,3}$	$\cdots$	$I_{z,3}$
$I_{y,1}$	$\pi/2$	$-I_{z,1}$			
$I_{y,2}$	$\pi/2$	$I_{z,2}$			
$I_{y,3}$	$\pi/2$	$-I_{z,3}$			
$I_{z,1}$	$\pi/2$	$I_{y,1}$			
$I_{z,2}$	$\pi/2$	$-I_{y,2}$			
$I_{z,3}$	$\pi/2$	$-I_{y,3}$			
	y Pulse			y Pulse	
$I_{x,1}$	$\pi/2$	$I_{z,1}$	$I_{z,1}$	$\pi/2$	$+I_{z,2}$
$I_{x,2}$	$\pi/2$	$-I_{z,2}$	$I_{z,2}$	$\pi/2$	$-I_{z,1}$
$I_{x,3}$	$\pi/2$	$-I_{z,3}$	$I_{z,3}$	$\cdots$	$I_{z,3}$
$I_{y,1}$	$\cdots$	$I_{y,1}$			
$I_{y,2}$	$\pi/4$	$-I_{y,3}$			
$I_{y,3}$	$\pi/4$	$I_{y,2}$			
$I_{z,1}$	$\pi/2$	$-I_{x,1}$			
$I_{z,2}$	$\pi/2$	$I_{x,2}$			
$I_{z,3}$	$\pi/2$	$-I_{x,3}$			

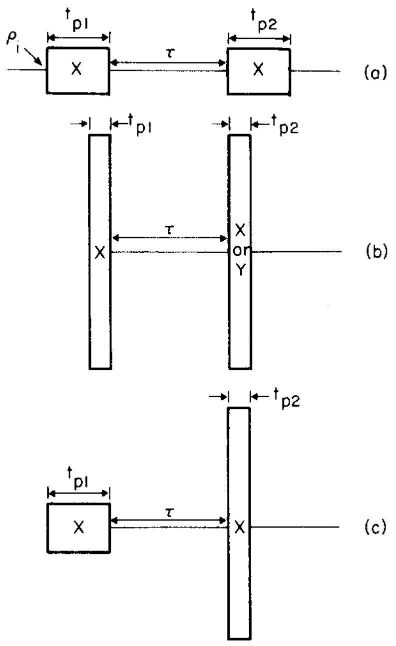

FIG. 20. Various pulse sequences used for preparation and detection of double quantum coherence. Pulse sequence (a) has two weak pulses. The first is to transfer $a_{z,1}$ to $a_{z,2}$, which then evolves during τ. The second transfers $a_{z,2}$ back to $a_{z,1}$, where it can then be detected by strong pulses yielding a signal proportional to the double quantum coherence $a_{z,2}(\tau)$. The pulses in (b) are stronger, yielding a mixture of double and single quantum effects. They are used to detect the amount of $a_{z,1}$ for example prepared by (a) by producing a spin echo at time 2τ proportional to $a_{z,1}$ before the pulses. This also overcomes the problem of detector recovery time. In (c) we see the simplest pulse sequence for monitoring the evolution of double quantum coherence. The signal after the second strong pulse is proportional to $a_{z,2}(\tau)$ as explained in the text.

$$\rho_i = I_{z,1},$$

$$\rho(t_p) \approx I_{z,1}\cos\frac{\omega_1^2}{\omega_Q}t_p - I_{z,2}\sin\frac{\omega_1^2}{\omega_Q}t_p,$$

$$\rho(t_p+\tau) \approx I_{z,1}\cos\frac{\omega_1^2}{\omega_Q}t_p - \sin\frac{\omega_1^2}{\omega_Q}t_p(I_{z,2}\cos 2\Delta\omega\tau - I_{z,3}\sin 2\Delta\omega t),$$

$$\rho(2t_p+\tau) \approx I_{z,1}\left(\cos^2\frac{\omega_1^2}{\omega_Q}t_p - \sin^2\frac{\omega_1^2}{\omega_Q}t_p\cos 2\Delta\omega\tau\right) - I_{z,2}\cos\frac{\omega_1^2}{\omega_Q}t_p\sin\frac{\omega_1^2}{\omega_Q}t_p(1+\cos 2\Delta\omega t) - I_{z,3}\sin\frac{\omega_1^2}{\omega_Q}t_p\sin 2\Delta\omega\tau,$$

where

$$t_p = t_{p1} = t_{p2}. \tag{81}$$

From this result we see that in the ideal case with $(\omega_1^2/\omega_Q)t_p = \frac{1}{2}\pi$, i.e., two 90° double quantum pulses:

$$\rho(2t_p+\tau) = -\cos 2\Delta\omega\tau I_{z,1} - \sin 2\Delta\omega\tau I_{z,3}, \tag{82}$$

and that *the coefficient of the final density matrix reflects the evolution of* $I_{z,2}$ between the pulses. When we

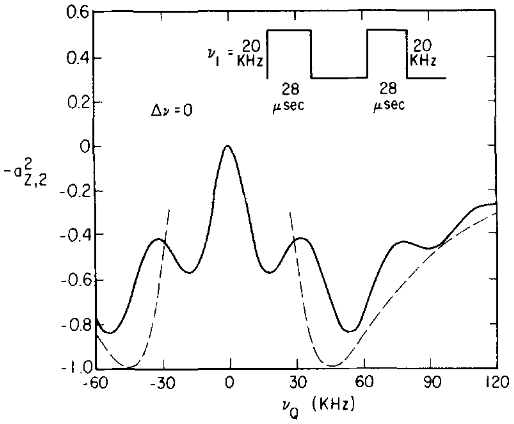

FIG. 21. Distortion in preparation and storage in $a_{z,1}$ of double quantum coherence by two weak pulse sequence for range of ω_Q values. The first pulse transforms $a_{z,1}$ to $a_{z,2}$ with an efficiency dependent on ω_Q. The second pulse stores $a_{z,2}$ at time τ back to $a_{z,1}$ (for subsequent detection) with the same efficiency. Thus the overall double quantum transfer function for this pulse sequence is proportional to $a^2_{z,2}$ where $a_{z,2}$ is calculated from one pulse as in Fig. 16. The solid line is an exact calculation and the dashed one is calculated for pure double quantum behavior $a^2_{z,2} = \sin^2(\omega_1^2/\omega_Q)t$.

have a distribution of ω_Q, e.g., in a powder, then of course we cannot satisfy the 90° double quantum pulse condition for all ω_Q. To see the distortion effects, the square of the exact coefficient of $a_{z,2}$ after the first pulse, which reflects the manner in which $I_{z,2}$ is created and "stored" as $I_{z,1}$, is shown with $\sin^2(\omega_1^2/\omega_Q)t_p$, for $\nu_1 = 20$ kHz and $t_p = 28$ μsec, as functions of ν_Q (Fig. 21). The advantage of storing the $a_{z,2}$ as $a_{z,1}$ with the second pulse is discussed in the next paragraph.

2. *Two strong pulses*

We go now over to the case in which we apply two strong rf irradiation pulses [Fig. 20(b)] on the spin system with a time delay of τ. This sequency is important for polycrystalline samples in which a range of ω_Q values are present. In that case this pulse sequence is used to obtain an echo signal since the amplitude of the signal following one pulse is obscured by dead time. If we consider an initial state $\rho_i = I_{z,1}$, then we obtain for the ω_Q and $\Delta\omega \ll \omega_1$ the following values: For

$$\omega_{1,x} t_{p1} = \tfrac{1}{2}\pi, \text{ and } \omega_{1,y} t_{p2} = \tfrac{1}{2}\pi,$$

$$a_{y,1}(t_{p1}) = 1, \text{ and } a_{y,1}(2\tau) = \cos^2\Delta\omega\tau, \qquad (83)$$

and for

$$\omega_{1,x} t_{p1} = \tfrac{1}{2}\pi, \text{ and } \omega_{1,x} t_{p2} = \tfrac{1}{2}\pi,$$

$$a_{y,1}(t_{p1}) = 1, \text{ and } a_{x,1}(2\tau) = \tfrac{1}{2}\sin 2\Delta\omega\tau, \qquad (84)$$

where we write $\rho(2\tau)$ for $\rho(t_{p1} + \tau + t_{p2} + \tau)$ and where $\omega_{1,p}$ is a pulse in the p direction. All other coefficients of $\rho(2\tau)$ are dependent on ω_Q and will average away for polycrystalline samples. From these results we see that the spin echo in a sample with a distribution of ω_Q is still dependent on $\Delta\omega$ while the ω_Q dependence essentially disappears. This effect will be discussed again in the next paragraph. In Fig. 22 an example of a two strong pulse sequence is shown with $\nu_1 = 60$ kHz and $t_{p1} = t_{p2} = 4$ μsec. The exactly calculated coefficient of $I_{y,1}$ after 2τ is plotted for different ν_Q values. The echo thus gives a good measure of $a_{z,1}$ before the two pulses.

3. *One weak pulse and one strong pulse*

The final two pulse sequence consists of one weak pulse followed after τ seconds by a strong pulse, Fig. 20(c). The reason for applying this sequence is to detect in the simplest way the coherence behavior during the delay time τ. If the first pulse is selected to be a double quantum 90° pulse, $(\omega_1^2/\omega_Q)t_{p1} = \frac{1}{2}\pi$, then the density matrix for $\rho_i = I_{z,1}$ is given after this pulse by

$$\rho(t_{p1}) = -I_{z,2}. \qquad (85)$$

The evolution of $\rho(\tau)$ during the time τ between the pulses is given by

$$\rho(t_{p1} + \tau) = -I_{z,2}\cos 2\Delta\omega\tau + I_{z,3}\sin 2\Delta\omega\tau, \qquad (86)$$

and the strong second detection pulse results in

$$\rho(t_{p1} + \tau + t_{p2})$$
$$= + I_{y,2}\cos 2\Delta\omega t + \tfrac{1}{2}[I_{x,3} - (I_{y,3} - I_{z,3})]\sin 2\Delta\omega\tau, \qquad (87)$$

where we took $\omega_1 t_{p2} = \frac{1}{2}\pi$ with $\omega_1 \gg \omega_Q$. This results in a signal intensity, according to Eqs. (79),

$$S_x = S_0 \cos 2\Delta\omega\tau \sin\omega_Q t \sin\Delta\omega t,$$

$$S_y = S_0 \cos 2\Delta\omega\tau \sin\omega_Q t \cos\Delta\omega t. \qquad (88)$$

The behavior of this pulse sequence is depicted schematically in Fig. 23 for $I_{y,1}$. The signal thus begins with zero intensity, but the average intensity during evolution after the second pulse is proportional to the double quantum free induction decay. A convenient way to detect the double quantum decay is to Fourier transform $S_x + iS_y$ and plot the intensity of the transform versus τ for the quadrupolar frequency of interest. A second Fourier transformation then yields the double quan-

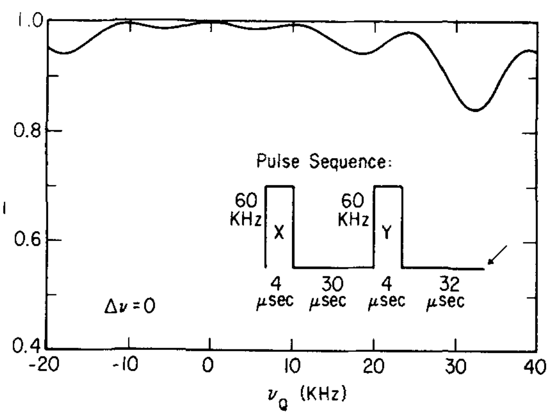

FIG. 22. Efficiency of detecting $a_{z,1}$ (created perhaps after two weak pulses) by two strong pulse sequence. The distortion induced by this sequence in detecting double quantum coherence will also contribute to the final line shape. The value of $a_{y,1}$, the detected signal at the arrow (near the echo maximum), is plotted as a function of ν_Q and shows very little distortion even for $\omega_Q = \frac{1}{2}\omega_1$.

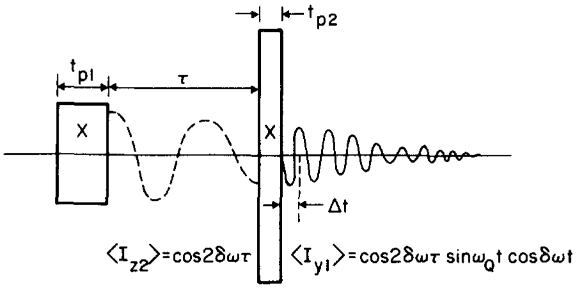

FIG. 23. Evolution and detection of double quantum coherence by simple two pulse sequence. The expressions on the figure are written for the ideal case of a pure double quantum $\pi/2$ pulse ($\omega_1 \ll \omega_Q$) followed by a normal single quantum $\pi/2$ pulse ($\omega_1 \gg \omega_Q$) starting with a density matrix $\rho_0 = I_z$. Fourier transformation of the signal yields a dispersionlike line with intensity proportional to $\langle I_{z,2}(\tau)\rangle = \cos 2\delta\omega\tau$.

tum spectrum. This is a special case of two-dimensional spectroscopy.[12] If there is a distribution of ω_Q as in a powder, the double quantum $\frac{1}{2}\pi$ condition cannot be met everywhere yielding characteristic line shapes.[13] This is discussed in the next section.

VII. EXAMPLES

In this last section we shall discuss some possible pulse sequences for the detection of the chemical shifts of spins with $I = 1$. The idea of detecting the coherence of the double quantum transition has been shown to be useful for the determination of chemical shifts values in single crystals and polycrystalline samples. The quadrupolar broadening is eliminated in the double quantum transition and the dipolar coupling can be eliminated by diluting the deuterium in a protonated host and spin decoupling the protons.

A. Single crystals

The fact that there are a finite number of discrete ω_Q values present in a measurement on a oriented single crystal makes it possible to detect the chemical shift value σ of a particular nucleus by a two pulse sequence as discussed at the end of the last section. In the ideal case in which we can apply pulses with either $\omega_1 \ll \omega_Q$ or $\omega_1 \gg \omega_Q$ the pulse lengths are determined by the conditions in the previous section. However, in practice it is not always possible to obtain these ideal pulses and we have to deal explicitly with the actual parameters (ω_1, t_p) of the pulses and the exact solutions for the density matrix and signal intensities. If we consider a deuterium nucleus in a crystal with a single well defined value ω_Q and we assume that the rf irradiation strength ω_1 always satisfies $\omega_1 \gg \delta\omega + \sigma\omega_0$, where $\delta\omega$ is the offset frequency of irradiation and σ is the unknown chemical shift (in ppm), we can derive the explicit expressions for the spin density matrix. The basic idea for the detection of σ is to apply two pulses; the first pulse to create the coherent state $I_{z,2}$ and the second to monitor it in the form of a signal. Consider as an example Fig. 20(c) using the simplest pulse sequence. The density matrix after the first pulse, applied to a spin system in thermal equilibrium, with intensity ω_1 and length $t_{p,1}$ is given by (not assuming $\omega_1 \ll \omega_Q$)

$$\begin{aligned}\rho(t_{p1}) = 2b\{&[\cos^2\theta/2 \cos\tfrac{1}{2}(\omega_e - \omega_Q)t_{p1} + \sin^2\theta/2 \cos\tfrac{1}{2}(\omega_e + \omega_Q)t_{p1}]I_{z,1}\\ &- [\cos^2\theta/2 \sin\tfrac{1}{2}(\omega_e - \omega_Q)t_{p1} - \sin^2\theta/2 \sin\tfrac{1}{2}(\omega_e + \omega_Q)t_{p1}]I_{z,2}\\ &+ \tfrac{1}{2}\sin\theta[\sin\tfrac{1}{2}(\omega_e + \omega_Q)t_{p1} + \sin\tfrac{1}{2}(\omega_e - \omega_Q)t_{p1}]I_{y,1} + \tfrac{1}{2}\sin\theta[\cos\tfrac{1}{2}(\omega_e + \omega_Q)t_{p1} - \cos\tfrac{1}{2}(\omega_e - \omega_Q)t_{p1}]I_{y,2}\},\end{aligned} \tag{89}$$

with

$$\omega_e^2 = 4\omega_1^2 + \omega_Q^2 \text{ and } \theta = \tan^{-1}(2\omega_1/\omega_Q).$$

The optimal preparation pulse makes the coefficient of $I_{z,2}$ one, i.e., $a_{z,2} = 1$. We require, therefore, that the $I_{y,1}$ and $I_{y,2}$ coefficients are zero, so as to make the signal intensities after this pulse zero. This condition becomes from (89)

$$\tfrac{1}{2}(\omega_e + \omega_Q)t_{p1} + \tfrac{1}{2}(\omega_e - \omega_Q)t_{p1} = 2\pi k, \tag{90}$$

i.e.,

$$t_{p1} = 2\pi k/\omega_e \quad k = 1, 2, \ldots \tag{91}$$

For this condition, Eq. (89) becomes

$$\begin{aligned}\rho(t_{p1}) = 2b[&\cos\tfrac{1}{2}(\omega_e - \omega_Q)t_{p1} I_{z,1}\\ &- \sin\tfrac{1}{2}(\omega_e - \omega_Q)t_{p1} I_{z,2}].\end{aligned} \tag{92}$$

In the ideal case we make the coefficient of $I_{z,2}$ equal to one in (92) by

$$\tfrac{1}{2}(\omega_e - \omega_Q)t_{p1} = \tfrac{1}{2}\pi(2n+1) \quad n = 0, 1, \ldots$$

Together with the definition of ω_e and Eq. (91) we obtain

$$t_{p1} = \frac{2m-1}{\omega_Q}\pi, \tag{93}$$

$$\omega_1 = \frac{1}{2}\left[\left(\frac{2k}{2m-1}\right)^2 - 1\right]^{1/2}\omega_Q \quad k, m = 1, 2, \ldots, \; k \geq m. \tag{94}$$

In Fig. 24 the values for t_{p1} and ω_1 are plotted as functions of ω_Q for $m = k = 1$ and $m = k = 5$. From such graphs we can determine appropriate ω_1 and t_p's for the experimental ω_Q. After this preparation pulse we let $\rho(t_{p1}) = 2bI_{z,2}$ evolve over a period of τ and apply the second pulse when

$$\begin{aligned}\rho(\tau) = 2bI_{z,2}&\cos 2(\delta\omega + \sigma\omega_0)\tau\\ &- 2bI_{z,3}\sin 2(\delta\omega + \sigma\omega_0)\tau.\end{aligned} \tag{95}$$

If we measure the signal intensity, S_y, Δt seconds after the second pulse and we take $\Delta t \ll 1/\delta\omega$, then any strong pulse gives an intensity proportional to $a_{z,2}(\tau)$

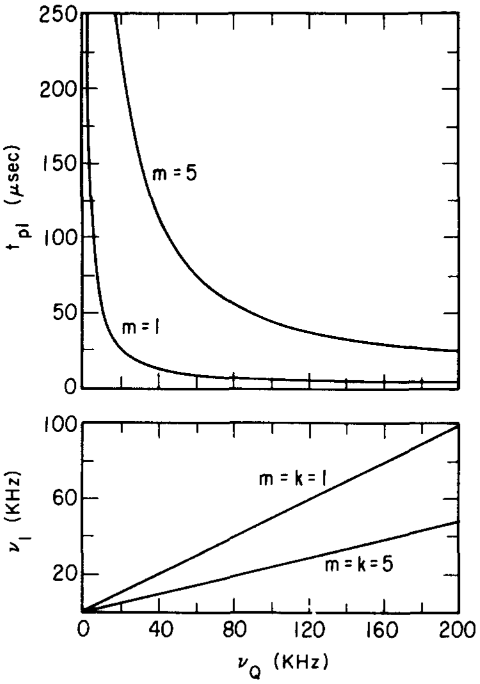

FIG. 24. Allowed values of t_{p1} and ν_1 as a function of ν_Q to produce pure 90° double quantum pulse from exact calculations. The integers k and m are defined in Eqs. (91)–(94) in the text.

$=2b\cos 2(\delta\omega+\sigma\omega_0)\tau$. The signal intensity after a second pulse in the x direction is seen from Table IV to be proportional to

$$S_x(\tau)\propto a_{z,3}(\tau), \tag{96}$$

and the proportionality factor is a function of the pulse length and height and of the value of ω_Q. In the ideal case of an infinitely strong x pulse we obtain for the S_y, t seconds after the pulse,

$$S_y(t)=S_0\cos 2(\delta\omega+\sigma\omega_0)\tau\sin\omega_Q t\cos(\delta\omega+\sigma\omega_0)t. \tag{97}$$

The double quantum decay can thus be plotted as a function of τ. The result after an arbitrary pulse can be written as

$$S_y(t)=S_0 a_y\cos 2(\delta\omega+\sigma\omega_0)\tau\sin(\omega_Q t+\phi), \tag{98}$$

where

$$a_y=(a_{y,1}(0)+a_{y,2}(0))^{1/2},$$

$$\phi=\tan^{-1}[a_{y,1}(0)/a_{y,2}(0)], \tag{99}$$

and $a_{y,1}(0)$ and $a_{y,2}(0)$ are the initial coefficients of $I_{y,1}$ and $I_{y,2}$ just after the second pulse. To demonstrate the dependence of a_y and ϕ on the parameters of the second pulse and on the value of ω_Q we show in Fig. 25 the exact calculated $a_{y,1}(0)$ and $a_{y,2}(0)$ values of the density matrix after a pulse of length $t_p=3\,\mu$sec and of height $\nu_1=60$ kHz applied on $\rho(\tau)=I_{z,2}$. It is clear that this projection of the density matrix on the y-coordinate system is strongly dependent on ω_Q and that the a_y and ϕ values in Eq. (98) are different for different ω_Q values.

1. Second order quadrupole shift

Before discussing some aspects of the double quantum coherence measurements on polycrystalline samples, we shall make some comments on the higher order corrections which we must consider in doing chemical shift measurements.

The quadrupole Hamiltonian as it was defined in Eq. (12) is only taken to first order with respect to the external magnetic field $-\omega_0 I_z$. There are, however, measurable second order effects, which will shift the measured ω_Q values by an amount

$$\omega_Q^{(2)}=(\omega_Q^2/12\,\omega_0)\,\tfrac{3}{8}(\sin^2 2\theta+\sin^4\theta) \tag{100}$$

with the definition of Eq. (12) and the assumption of a symmetric quadrupole tensor. A straightforward calculation shows that this correction adds up to the Hamiltonian in the rotating frame as

$$\mathcal{H}=-2(\delta\omega+\sigma\omega_0)I_{z,1}+2\omega_Q^{(2)}I_{z,1}+\tfrac{2}{3}\omega_Q(I_{x,3}-I_{y,3}).$$

This result shows us that this second order correction is indistinguishable from the chemical shift tensor and that it must be calculated and subtracted from the measured value $\sigma\omega_0+\omega_Q^{(2)}$. In a magnetic field of ~4.5 T the correction can introduce a shift in σ of the order of 1 ppm for ω_Q ~100 kHz. We now go over to discuss some aspects of measurements on polycrystalline samples.

B. Polycrystalline samples

In this paragraph we discuss the measurements of the chemical shielding tensor in polycrystalline samples. The distribution of ω_Q values in a powder sample complicates the detection of the chemical shift pattern as depicted schematically in Fig. 26. In particular, as was discussed in the former sections, the preparation of the double quantum coherence and its detection is strongly dependent on the quadrupolar frequency ω_Q. The simplest pulse sequence for the detection of $\sigma\omega_0$ is the two pulse sequence shown in Fig. 20(c). After the first pulse we obtain a value of the coefficient of $I_{z,2}$ which will now be ω_Q dependent, $a_{z,2}(\omega_Q)$. In

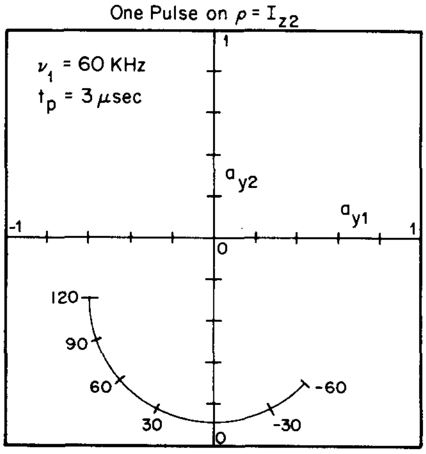

FIG. 25. Application of single pulse of intensity $\nu_1=60$ kHz and duration 3 μsec applied to $\rho(\tau)=I_{z,2}$. Shown are the values of $a_{y,1}$ and $a_{y,2}$ on the circular arc as a function of ν_Q. This demonstrates the distortion in amplitude a_y and phase ϕ from Eqs. (98) and (99) in detecting the double quantum coherence with sequence 20(c).

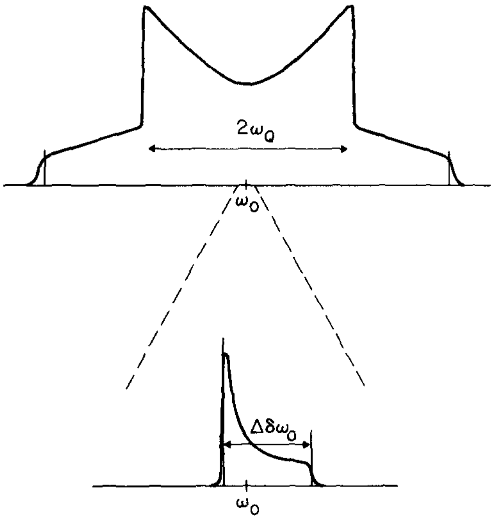

FIG. 26. Schematic representation of powder pattern for deuterium with axially symmetric electric field gradient and chemical shift terms. We wish to determine the chemical shift anisotropy which is broadened tremendously by the quadrupolar splittings.

the ideal case we would like to obtain $a_{z,2}(\omega_Q)\approx 1$, but this is not possible practically over the whole ω_Q range. We therefore apply a first pulse which will make $a_{z,2}(\omega_Q)$ maximum over the range of ω_Q's. The optimization can be determined by a high speed computer calculation and these procedures will not be discussed here. In Fig. 16 an $a_{z,2}(\omega_Q)$ plot is shown for the case of one pulse with a maximum value of $\nu_Q = 120$ kHz. Except for the values of ν_Q near $\nu_Q = 0$, the $a_{z,2}(\omega_Q)$ values are larger than 0.6, if we take $\rho_i(\omega_Q) = I_{z,1}$. To obtain the efficiency of the detection of the double quantum coherence $Q(\tau, \omega_Q)$, we calculate the observable $a_{y,1}(\omega_Q)$ after the second x pulse originating from $a_{z,2}(\omega_Q)$ just before this pulse. *The product of $a_{z,2}(\omega_Q)$ after the first pulse and this $a_{y,2}(\omega_Q)$ will yield the efficiency of the measurement of double quantum coherence for the different ω_0 values. We shall call this product the double quantum transfer function.* Again, in the ideal case this transfer function would be one over the whole ω_Q range. In Fig. 27(a) we show a transfer function of a two pulse sequence calculated for $a_{y,1}$ just after the second pulse. This illustrates the type of distortion which will be obtained in the Fourier transform double quantum spectrum as a function of ω_Q. We shall of course have for every function a value of zero for $\omega_Q = 0$. Knowing the transfer function we are able to predict the high resolution spectrum for an experiment where the total signal

$$S_y = \int_{\text{all } \omega_Q} d\omega_Q a_{y,1}(\omega_Q)$$

is measured just after the second pulse as a function of the time between the pulses, τ. We need, however, to know the relative orientations of the electric quadrupole tensor and the chemical shielding tensor.

Before we show an actual calculation of a high resolution double quantum chemical shift powder spectrum, we realize that in practice S_y cannot be obtained just after the second pulse due to detector recovery time. In Fig. 27(b) we show again the transfer function for the same conditions as in Fig. 27(a), if we wait 30 μsec to detect S_y after the second pulse due to receiver dead time. Due to the ω_Q dependence of $a_{y,1}$ after the pulse we do not obtain a useful transfer function and we are forced to use other pulse sequences. A good example for detection of the double quantum decay is the pulse sequence of Fig. 20(a). With this sequence we store the $a_{z,2}(\omega_Q)$ coefficients in the coefficients of $I_{z,1}$. This was discussed in the last section and a calculated $a_{z,1}(\omega_Q)$ after the second pulse is shown in Fig. 21. If we wait now more than T_2 seconds and we apply a third pulse the signal S_y will be proportional to the coherence $a_{z,2}$ before the second pulse, i.e., will map out the double quantum decay. In Fig. 28(a) the transfer function for this kind of experiment is shown. Again optimization techniques must be used to obtain the best maximum transfer function; comparing Fig. 27(a) and Fig. 28(a), we see that the first result is somewhat favorable over the second, although we realize that the rf irradiation strength is not much larger than ω_Q and that therefore $a_{y,1}$ is generated instead of $a_{y,2}$. To overcome the problem of not being able to measure S_y just after the strong pulse, we combine the pulse sequences of Fig. 20(a) with 20(b). In combining these two sequences we obtain an echo signal after the fourth pulse which has an amplitude almost equal to the value of S_y just after the third pulse. The corresponding

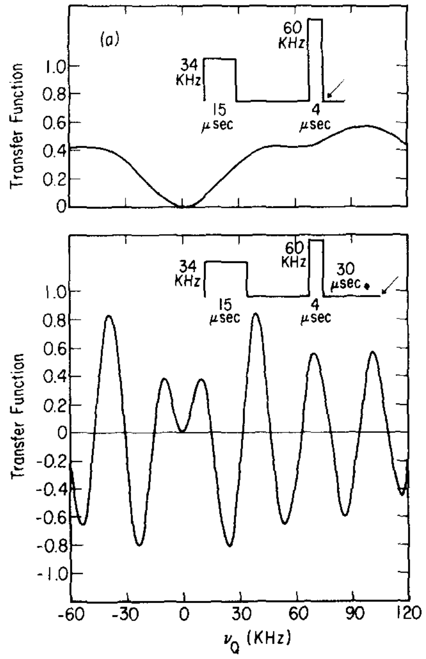

FIG. 27. Double quantum transfer function, i.e., detected signal $a_{y,1}$ at position of arrow for two pulse sequence. The first weak pulse prepares the double quantum coherence and the second stronger one monitors the decay. The line shape shows the type of distortion across the ν_Q values for realistic and optimal values of the parameters. In (a) the signal intensity is calculated immediately after the pulse. Since this practically is impossible, (b) shows the effect of detecting after 30 μsec. The distortion would make this essentially useless for application to a powder. This can be alleviated using an echo.

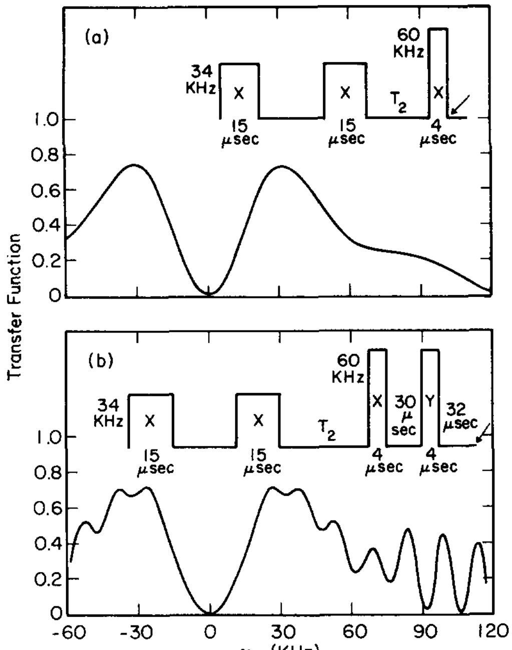

FIG. 28. Detected signal $a_{y,1}$ at position of arrow for three and four pulse sequences. (a) Shows the detection of double quantum coherence prepared and stored by two weak pulses. In (b) the practically more useful case of a spin echo is shown. This shows that an appreciable amount of double quantum coherence is prepared and detected over the whole ν_Q range.

transfer function for this four pulse sequence is shown in Fig. 28(b) and can be compared with the results of Fig. 29(a). These results are indeed very good if we realize that the irradiation strength was much smaller than the extreme ω_Q values.

To calculate the expected polycrystalline chemical shift line shape from the double quantum decay for the pulse sequence of Fig. 28(b) we assume as a simple example that the electric field gradient tensor and the chemical shift tensor are axially symmetric with their symmetry axes parallel. The result is shown in Fig. 29(a) and is compared with the real line shape function that we should have measured if there were no quadrupole interaction in the powder sample. In Fig. 29(b) we show a similar result for the two pulse sequence. These theoretical results show that it is indeed possible to detect high resolution double quantum spectra from polycrystalline samples and that by choosing the proper pulse sequences all information about the chemical shielding can be obtained. In practice the results of Figs. 28 and 29 will be broadened and part of the complicated line shape will not be observable. It is also clear that for other relative orientations of the quadrupole and the shielding tensor the distortion of the double quantum spectrum will be different, so that from the line shape we can say something about the relative orientations of the electric field gradient and shielding tensors. Experimental results on polycrystalline samples will be shown in a separate paper.[13]

C. Double quantum phase shift and spin locking

We saw in Sec. III that irradiating the spin-1 system near ω_0 with a field $-\omega_1 I_x$ such that $\omega_1 \ll \omega_Q$ was effectively equivalent to irradiating it in the double quantum frame with $-(\omega_1^2/\omega_Q)I_{z,3}$. In fact, the effective double quantum operator from Eq. (44) can be written

$$\mathcal{H}_{DQ} \simeq -2\delta\omega I_{z,1} - (\omega_1^2/\omega_Q) I_{z,3} \qquad (101)$$

ignoring the commutative quadrupole term. The effective rf field is along the $z, 3$ axis in this frame. We now enquire about the effect of the rf phase on the direction of ω_1^2/ω_Q in the double quantum frame. To do this we assume that an rf field is applied with arbitrary phase ϕ, i.e., the rotating frame Hamiltonian has the form

$$\mathcal{H} = -2\delta\omega I_{z,1} - 2\omega_1(I_{x,1}\cos\phi + I_{y,1}\sin\phi). \qquad (102)$$

Applying the same transformation as in Eq. (42) and assuming again $\omega_1 \ll \omega_Q$ we find to a good approximation the effective double quantum Hamiltonian

$$\mathcal{H}_{DQ} \approx -2\Delta\omega I_{z,1} - (\omega_1^2/\omega_Q)(I_{z,3}\cos 2\phi + I_{z,2}\sin 2\phi), \qquad (103)$$

where again the commutative term $\frac{2}{3}\omega_Q(I_{x,3} - I_{y,3})$ has been dropped. *Thus an rf phase shift of* ϕ *corresponds to a shift of* 2ϕ *in the double quantum frame.* For example, a phase shift of 90° causes the effective transverse double quantum field to reverse sign. A phase shift of 45° would be used to effect double quantum spin locking. This would be done by applying a 90° double quantum pulse $(\omega_1^2/\omega_Q)t = \frac{1}{2}\pi$ transforming the density matrix from $I_{z,1}$ to $I_{z,2}$ and then phase shifting by 45° inducing spin locking of the density matrix by the operator $(\omega_1^2/\omega_Q)I_{z,2}$. The phase effects are summarized schematically in Fig. 30.

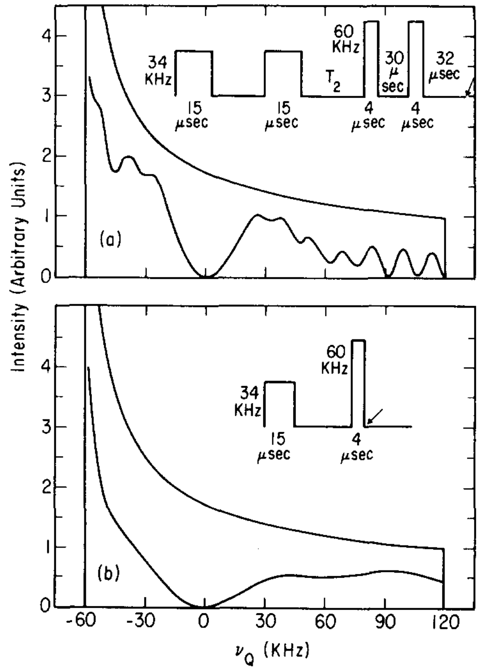

FIG. 29. Calculated Fourier transform double quantum spectra for polycrystalline deuterium sample with axially symmetric electric field gradient and chemical shift tensors having their symmetry axes parallel. The spectrum is obtained by multiplying the ideal chemical shift powder pattern (top solid line) by the functions for the corresponding pulse sequences in Figs. 28(b) and 27(a).

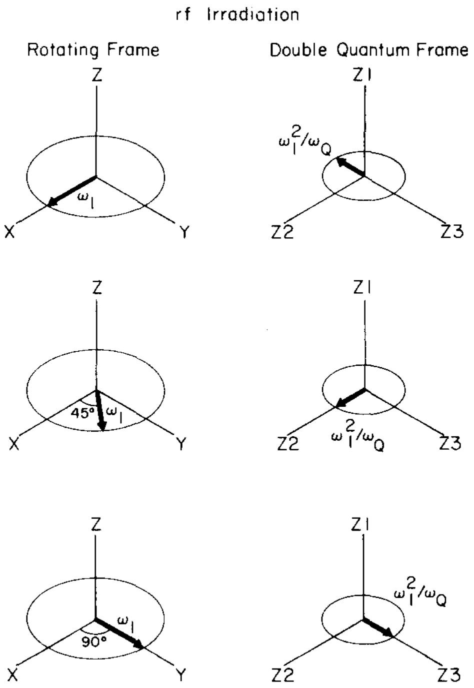

FIG. 30. Effect of rf phase on the double quantum phase. A phase shift of ϕ for ω_I in the rotating frame corresponds to a 2ϕ shift for the effective field ω_I^2/ω_Q in the double quantum frame. The absolute phases in each frame are arbitrary and were taken only for convenience of presentation.

Both phase reversal and spin locking experiments have been performed successfully and the results are presented elsewhere.[14]

ACKNOWLEDGMENTS

We are indebted to T. W. Shattuck and J. Murdoch for assistance with the calculations and to Professor E. L. Hahn and Professor R. A. Harris for some most interesting and valuable discussions.

---

[*] Support of this work by the U.S. Energy Research and Development Administration, the National Science Foundation, and the Petroleum Research Fund administered by the American Chemical Society is gratefully acknowledged.

[†] Present address: Division of Isotope Research, Weizmann Institute of Science, Rehovot, Israel.

[‡] Alfred P. Sloan Foundation Fellow and Camille and Henry Dreyfus Teacher Scholar.

[1] (a) C. P. Slichter, *Principles of Magnetic Resonance* (Harper and Row, New York, 1963); (b) A. Abragam, *Principles of Nuclear Magnetism* (Oxford U. P., Oxford, 1961).

[2] A. Pines, D. J. Ruben, S. Vega, and M. Mehring, Phys. Rev. Lett. **36**, 110 (1976); S. Vega, T. W. Shattuck, and A. Pines, Phys. Rev. Lett. **37**, 43 (1976).

[3] H. Hatanaka, T. Terao, and T. Hashi, J. Phys. Soc. Jpn. **39**, 835 (1975); T. Hatanaka and T. Hashi, J. Phys. Soc. Jpn. **39**, 1139 (1975).

[4] R. G. Brewer and E. L. Hahn, Phys. Rev. A **11**, 1641 (1975).

[5] S. Vega, J. Chem. Phys. **63**, 3769 (1975); S. Vega (to be published).

[6] W. R. Frazer, *Elementary Particles* (Prentice Hall, New Jersey, 1966); T. W. Shattuck, Ph.D. thesis, Berkeley, 1976. This also describes the application of double quantum concepts and experimental techniques to high resolution deuterium *nmr* in solids and double quantum cross polarization. A similar definition of $SU(3)$ operators in the basis of I_t is also possible.

[7] R. P. Feynman, F. L. Vernon, and R. W. Hellwarth, J. Appl. Phys. **28**, 49 (1957).

[8] W. de Boer, Phys. Rev. B **12**, 828 (1975).

[9] B. C. Sanctuary, J. Chem. Phys. **64**, 4352 (1976); E. Arimondo and G. Moruzzi, J. Phys. B **9**, 723 (1976).

[10] A. G. Redfield, Phys. Rev. **98**, 1787 (1955); W.-K. Rhim, A. Pines, and J. S. Waugh, Phys. Rev. B **3**, 684 (1974).

[11] J. S. Waugh (private communication).

[12] W. P. Aue, E. Bartholdi, and R. R. Ernst, J. Chem. Phys. **64**, 2229 (1976).

[13] S. Vega, D. E. Wemmer, and A. Pines (to be published).

[14] S. Vega and A. Pines, Proc. 19th Ampère Congress, Heidelberg, 395 (1976).